CHALMERS

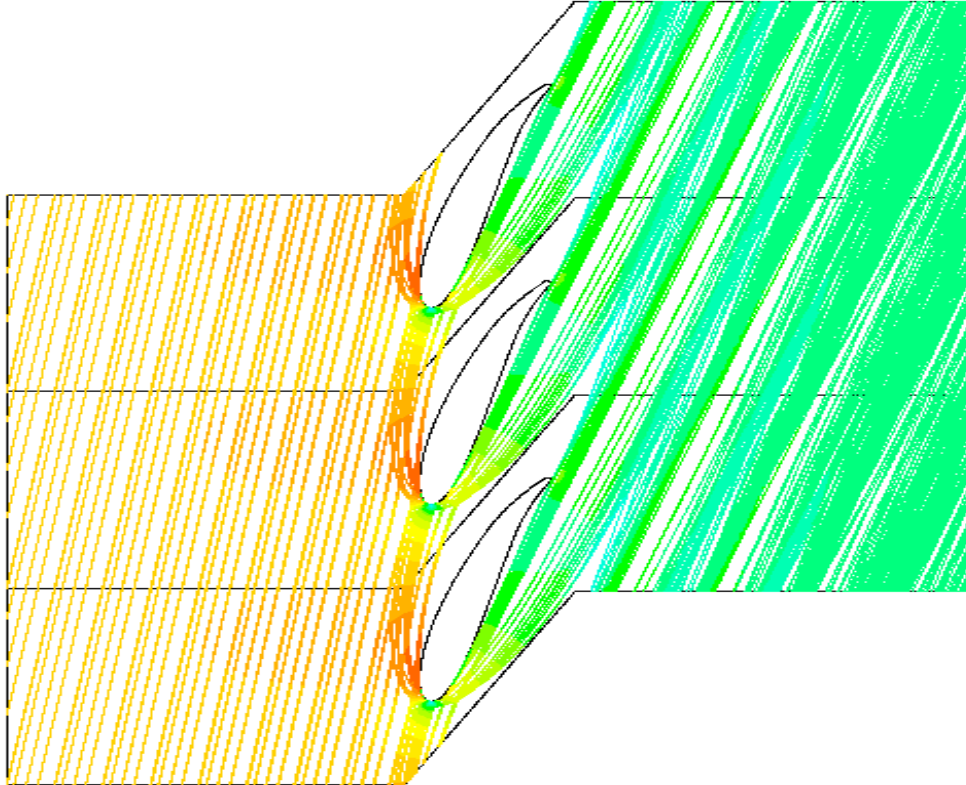## UNIVERSITY OF TECHNOLOGY

Effect of Different Oil Droplet Sizes in a Flow of Natural Gas around a Compressor Blade

Numerical Simulations of Multiphase Flow using Computational Fluid Dynamics

Master's thesis in Innovative and Sustainable Chemical Engineering
& Sustainable Energy Systems

KAJSA NOHLÅS
SIGNY TRYGGVADOTTIR

Department of Applied Mechanics
CHALMERS UNIVERSITY OF TECHNOLOGY
Gothenburg, Sweden 2015

Effect of Different Oil Droplet Sizes in a Flow of Natural Gas around a Compressor Blade

Numerical Simulations of Multiphase Flow using Computational Fluid Dynamics

KAJSA NOHLÅS

SIGNY TRYGGVADOTTIR

Department of Applied Mechanics
Division of Fluid Dynamics
CHALMERS UNIVERSITY OF TECHNOLOGY
Gothenburg, Sweden 2015

Effect of Oil Droplet Sizes in a Flow of Natural Gas around a Compressor Blade
Numerical Simulations of Multiphase Flow using Computational Fluid Dynamics
KAJSA NOHLÅS
SIGNY TRYGGVADOTTIR

Cover: Particle tracks, colored by velocity magnitude, for three blades in the initial
blade passage of a wet gas compressor, constructed in Fluent.

Effect of Different Oil Droplet Sizes in a Flow of Natural Gas around a Compressor Blade
Numerical Simulations of Multiphase Flow using Computational Fluid Dynamics
KAJSA NOHLÅS
SIGNY TRYGGVADOTTIR
Department of Applied Mechanics
Chalmers University of Technology

Abstract

Subsea is a term that refers to drilling and processing of gas and oil in underwater locations. One example of a subsea technology is a wet gas compressor which is used to compress fluids that consists of multiple phases. By compressing the wet gas the recovery of unprocessed streams can be increased and the investment cost reduced. The Norwegian company OneSubsea has designed and manufactured a wet gas compressor, first of its kind, and is developing the next generation of the compressor with assistance from the technical consultancy company ÅF. At ÅF's department for technical analysis in Gothenburg simulations of the compressor with pure gas flow are performed. To compliment these simulations a separate project is performed to evaluate the effects of a flow that is multiphase. Therefore the aim of this project is to study the effect of different droplet sizes on a gas flow around a compressor blade in a wet gas compressor.

Multiphase flow, consisting of natural gas and oil droplets, around one blade in the first step of the wet gas compressor is considered. Computational fluid dynamic simulations of one way coupled multiphase flow are solved using the conservation equations of mass and momentum, Lagrangian particle tracking and the $k - \omega$ SST turbulence model. The range of the droplet size and volume fraction evaluated are 1-200 µm and 1-2%, respectively.

Several different studies were performed. The results are characterised by flow properties outputted just after the blade, at the start of the next blade row, and with visualisations of the particle tracks around the blade. The main study, the Base case, consisted of 22 different case studies where the droplet size was held constant for each case, but varied within the size range between the cases. A coefficient of restitution (COR) was used to model the droplet wall interaction and the results showed that the droplets have an effect on the outflow from the first compressor step. The droplets decrease the average velocity angle at the axial clearance for all droplet sizes. The decrease is low, at a relatively constant value, for droplet sizes up to around 80 µm. For droplets larger than 80 µm, velocity angle decreases with increasing droplet size. By studying the particle tracks around the blade the droplet flow could be divided into three characteristic regions, according to the importance of wall interaction and effect of gas flow on the droplet.

After analysing the results from the Base case the importance of wall interaction was studied further. Simulations showed that the majority of the droplets are colliding with the wall. A sensitivity study for the COR was performed which showed that the droplet flow is independent of COR for droplet sizes up to 50 µm, almost independent up to 100 µm, and strongly dependent for the rest of the size range. A case study where the droplets were trapped at the wall was performed, but the reliability of these results are questionable since the data is based on a small fraction of droplets that pass the blade. For the final wall interaction study a liquid wall film at the blade was modelled. According to the theory this should be the most realistic way to model a droplet wall interaction. Due to lack of time this case study could not be fully completed and only an idea of the result is presented. The result shows that a thin film will cover the blade which has an effect on the particle tracks.

The conclusion from this project is that the droplets will effect the flow around the blade by decreasing the average velocity angle for the flow entering the next blade row; the magnitude of the effect is increasing with increased droplet size. The droplet wall interaction is important for the particle tracks, thus it is recommended to further evaluate this aspect.

Acknowledgements

Nomenclature

Abbreviations

CFD	Computational Fluid Dynamics
COR	Coefficient of Restitution
LPT	Lagrangian Particle Tracking
MWAVA	Mass Weighted Average Velocity Angle
RANS	Reynolds Averaged Navier Stokes
SST	Shear Stress Transport

Symbols

Variable	Unit	Description
Re	-	Reynolds number
ρ	kg/m^3	Density
U	m/s	Flow velocity
L	m	Flow length scale
μ	$kg/(s \cdot m)$	Viscosity
x	m	Location
τ	Pa	Stress tensor
t	s	Time
h	J	Total energy
h_n	J	Enthalpy
j_n	$mol \cdot /(m^2 \cdot s)$	Diffusion flux
k_{eff}	-	Conductive constant
S	$1/m^3$	Source term
T	K	Temperature
m	kg	Mass
ν	m^2/s	Kinematic viscosity
$\langle u_i u_j \rangle$	m^2/s^2	Reynolds stress
k	J/kg	Turbulent kinetic energy
ε	J/kg	Energy dissipation rate
ω	J/kg	Specific dissipation
y^+	-	First cell distance from wall
u_*	-	Wall friction velocity
l_*	-	Characteristic wall length scale
β^*	-	Constant
σ	-	Turbulence model constant
μ_t	$kg/(s \cdot m)$	Turbulent eddy viscosity
P_k	J/kg	Production rate of turbulence
F	-	Blend factor

a_1	-	Constant
Ω	-	Vorticity magnitude
d	m	Distance to the nearest wall
ϕ	-	Constant
γ	-	Constant
β	-	Constant
α	-	Volume fraction
V	m^3	Volume
N	-	Total number
v	m/s	Continuous phase velocity
u	m/s	Dispersed phase velocity
St	-	Stokes number
τ	s	Response time
d	m	Diameter
F	N	Forces
A	m^2	Projected area
C_D	-	Drag coefficient
P	$kg/(m \cdot s^2)$	Pressure
τ	$kg/(m \cdot s^2)$	Shear force
g	m/s^2	Gravity
ε	-	Coefficient of restitution
ϵ	-	Globalised coefficient of restitution
β	-	Viscous effect of film drainage
h	m	Film height
$\vec{V}$	m/s	Mean film velocity
$\dot{m}_s$	kg/s	Mass source
E	$kg \cdot m^2/s^2$	Impact energy
δ_{bl}	-	Boundary layer thickness
CFL	-	Courant number
Δt	s	Time step
σ	N/m	Surface tension

Index

Variable	Description
n	Species
d	Dispersed phase
c	Continuous phase
imp	Impact
res	Resulting
max	Maximum
b	Boiling

Contents

Contents

List of Figures

List of Tables

1

Introduction

In this chapter the background for the project is introduced as well as the aim and constraints. Also a compact presentation of the method is provided.

1.1 Background

Subsea is a term that refers to drilling and processing of gas and oil in underwater locations, and is a key technology in the offshore gas- and oil market. One example of a subsea technology is a wet gas compressor which is used when the flow consists of multiple phases, i.e. the flow does not consist only of pure gas but also of different contaminants. In the compression of natural gas in a subsea system these contaminants can be water, oil, sand etc.. By compressing the wet gas using subsea technology the recovery of unprocessed streams can be increased and the investment cost can be reduced, compared to when traditional compression methods are used [13].

OneSubsea is a Norwegian technology company that delivers integrated solutions, products, systems and services for the subsea gas- and oil market. OneSubsea is a leading company in this field and offers its own wet gas compressor design, the very first of its kind, based on a technology that has been developed over the past 25 years. The company's multiphase wet gas compressor, WGC4000, is counter-rotating and its design is based on a hydraulic and mechanical design for boosting the pressure of an unprocessed well stream. An illustration of the exterior design is presented in Figure 1.1 [13].

At present, OneSubsea is developing the next generation of their wet gas compressor, WGC6000. This compressor will have larger capacity and higher performance than its predecessor. One essential part of the development process is the design of the compressor blade, which OneSubsea has asked ÅF, a leading Swedish company in technical consulting, to assist with. Calculations on the compressor design are performed at ÅF's department for technical analysis and the model used is based on an assumption of pure gas, i.e. neglecting the effect of wet gas. To compliment this project a separate study is performed, that aims at evaluating the wet gas effect on the flow around the compressor blade, by simulating oil droplets in natural gas flow using computational fluid dynamics (CFD). These are the first muliphase flow simulations performed on this wet gas compressor.

Figure 1.1: Illustration of the exterior design of the wet gas compressor WGC4000.

1.2 Aim

The aim of the project is to study the effect of different droplet sizes in a multiphase flow around a compressor blade in a wet gas compressor used in a subsea system. The objective is to provide OneSubsea with an increased understanding of the effect that the presence of wet gas has on their compressor. Ideally this will be done by finding a simple representation of how the different droplet sizes affect the total outflow.

1.3 Constraints

The following constraints are defined for the project.

- The design of the compressor blade is based on the design provided by One-Subsea.

- The domain will be two dimensional, non rotating and consists of one blade of the initial blade passage in the compressor, according to request from One-Subsea.

- The variable of interest is particle size, therefore the rest of the properties of the flow will be held constant.

- The software package ANSA 15.2 (ANSA) is used to create the computational domain.

- The software packages ANSYS CFX 15.0 (CFX) and ANSYS 15.0 (Fluent) are used for the CFD simulations.

Important to note is that the aim of this study is not to evaluate the difference in performance for the two CFD software packages. Two programs are used to give

the students the opportunity to develop their skills in both programs, instead of just one. Nevertheless, it will make it possible for the students to identify possible weaknesses and strengths for each program throughout the process, which can be useful in future studies.

1.4 Method

A literature study of multiphase flow and other relevant areas was performed. A computational domain, based on the geometric information provided by OneSubsea, was created in ANSA. The models used to represent the wet gas flow were chosen. Numerical calculations were performed in the software package ANSYS 15.0, including Workbench, Fluent, CFX and CFD Post. The resulting data was processed and analysed.

2

Theory

In this section the theory behind this study is explained. Initially the basics for describing fluid flow will be presented, including the characteristics of turbulent flow and how to model it. This is followed by a section defining multiphase flow and some parameters that are essential for characterising it. Different methods for how to model a multiphase flow is presented. Finally the chapter ends with a section presenting CFD and a stepwise guide of how to perform a typical CFD simulation.

2.1 Fluid flow

Fluid flow is a flow of either a gas or a liquid where shear stress is the main cause of the fluid motion. Flow can either be steady or unsteady. Steady flow occurs where the flow variables at a given point do not change with time. Unsteady flow is where these variables change with time [5].

In fluid mechanics dimensionless numbers, such as the Reynolds number, are often used to describe certain behavior of the fluid. The Reynolds number is defined as

$$Re = \frac{\rho U L}{\mu} \tag{2.1}$$

where U and L are the characteristic velocity and length scale of the flow and ρ and μ are the flow density and viscosity [15]. Reynolds number, Re, is used to determine whether the flow is laminar or turbulent. In laminar flow the layers of the fluid move smoothly with respect to each other, which is characterized by low Reynolds number and often low velocity. Turbulent flow is where mixing of the fluid occurs due to turbulence that leads to a change in flow variables at a given point in time. High Reynolds number indicates turbulent flow [5].

2.1.1 Governing equations

Fluid flow can be described using conservation equations, called governing equations, which describe the conservation of mass, momentum and energy. Their general form is derived from Reynolds' transport theorem which shifts the solution of the governing equations from using a system concept, collection of matter of fixed identity, to control volume concept, volume in space which fluid flows through. It relates two different reference frames; the Eulerian reference frame, where the coordinates are

fixed and the fluid is observed as it passes by, and the Lagrangian reference frame, where a moving fluid element is followed [15]. The general form of the flows governing equations are stated in (2.2), (2.3) and (2.4). The equations are coupled, partial, nonlinear differential equations and in this study they are presented in tensor form [1].

The governing equations are derived for a continuum. In a fluid flow the parameters of the flow vary continuously from point to point and a continuum is satisfied when a point volume is reached, where the parameters stop varying and become a constant value, and when that point volume is smaller than the size of the domain [6].

The mass conservation equation is called the continuity equation and states that the mass of a system is constant. The tensor form of the continuity equation over a stationary fluid element, $\Delta x_1 \Delta x_2 \Delta x_3$, is presented in (2.2) where Δx_1, Δx_2 and Δx_3 are the lengths of the fluid element in each dimension; in this case three dimensions [1, 15].

$$\frac{\partial \rho}{\partial t} + \frac{\partial \rho U_j}{\partial x_j} = 0 \tag{2.2}$$

In (2.2) x_j represents the location in time and U_j is the velocity of the flow for $j = [1, 2, 3]$ [1].

The momentum conservation equation is a result of Newton's second law, which states that the rate of momentum change is equal to the forces acting on a body. The momentum equation in a tensor form over a fluid element $\Delta x_1 \Delta x_2 \Delta x_3$ is

$$\frac{\partial U_i}{\partial t} + U_j \frac{\partial U_i}{\partial x_j} = -\frac{1}{\rho}\frac{\partial P}{\partial x_i} + \frac{1}{\rho}\frac{\partial \tau_{ij}}{\partial x_j} + g \tag{2.3}$$

where the stress tensor, τ, is defined as $\tau_{ij} = \tau_{ji} = \mu\left(\frac{\partial U_i}{\partial x_j} + \frac{\partial U_j}{\partial x_i}\right)$ and $i, j = [1, 2, 3]$. This results in three equations, one in each direction of the three dimensional space, which is the definition of the Navier-Stokes equations. It is common that the continuity equation is included along with these three equations when referring to the Navier-Stokes equations [1, 15].

The tensor form of the energy conservation equation describes the rate of change in the flow within a certain system [5].

$$\frac{\partial h}{\partial t} = -\frac{\partial}{\partial x_j}\left[hU_j - k_{eff}\frac{\partial T}{\partial x_i} + \sum_n m_n h_n j_n - \tau_{kj}U_k\right] + S_h \tag{2.4}$$

where h is the total energy composed of kinetic, thermal, chemical and potential energy, T is temperature, m is mass, h_n and j_n are the standard state enthalpy and the diffusion flux, respectively, of species n, k_{eff} is a conductive constant and S_h is a general source term [1].

2.1.2   Turbulent flow modelling

Turbulent flow is commonly found in industrial applications; in fact most flows are turbulent by nature. Thus models describing turbulent flow are essential when modeling fluid flow.

Turbulent flow is very irregular and the fluctuations in flow variables make time and length scales incoherent. Turbulent flow is characterised by velocity fields with small scaled, high frequency fluctuations and an enormous amount of information is needed to solve a turbulent flow completely. This makes it computationally expensive to solve turbulent flow, compared to laminar flow. To be able to represent these type of flows the governing equations can be manipulated to remove the small scaled, high frequency fluctuations. These manipulations result in addition of unknown variables. To model these variables turbulence models are used, thus turbulence models can be seen as a closure for the governing equations for turbulent flows [1].

There are many different turbulence models available. The models are ranging in approximation level and applications. The most exact ones, such as direct numerical simulation and large eddy simulations, are normally too computationally expensive to use for industrial applications [1].

Most turbulence models applicable in engineering are based on the Reynolds decomposition concept. It proposes that the instantaneous variables can be split into two different parts: one mean part and one fluctuating part. When this concept is applied to the Navier-Stokes equation it results in a set of equations called the Reynold Averaged Navier-Stokes equations (RANS) which are presented in (2.5) for continuity and momentum [1].

$$\frac{\partial \langle U_j \rangle}{\partial x_j} = 0$$

$$\frac{\partial \langle U_j \rangle}{\partial t} + \langle U_j \rangle \frac{\partial \langle U_i \rangle}{\partial x_j} = \frac{1}{\rho} \frac{\partial \langle P \rangle}{\partial x_i} + \nu \frac{\partial \langle U_i \rangle}{\partial x_j^2} - \frac{\partial \langle u_i u_j \rangle}{\partial x_j} \tag{2.5}$$

In the RANS equations, variables enclosed with $\langle \ \rangle$ define the mean part of the variable and ν is the kinematic viscosity, defined as $\nu = \frac{\mu}{\rho}$. The term $\langle u_i u_j \rangle$ is referred to as the Reynolds stresses, for which the exact definition is $-\rho \langle u_i u_j \rangle$. The Reynolds stresses describe the transfer of momentum by turbulence and since it consists of products of the velocity fluctuations it introduces an unknown variable into the equation. Thus, applying the Reynolds decomposition concept to the Navier-Stokes equations results in an additional term, without the addition of an equation. Therefore the modelling of this term, i.e the Reynold stresses, is the core purpose of the turbulence models that uses the RANS equations [6].

The turbulence models based on the RANS equations can be classified as zero-, one- or two- equation models. The number refers to the number of differential equations used to model the Reynold stresses, in addition to the RANS equations. The two-

equation models are the most common ones, since they are robust and inexpensive to implement [1].

2.1.2.1 Two-equation turbulent models

Two popular two equation models are the $k - \varepsilon$ and $k - \omega$ models. k is defined as turbulent kinetic energy and the two length scales ε and ω are defined as energy-dissipation rate and specific dissipation, respectively. Since the models consist of two equations the length scale can be determined independent of the turbulent kinetic energy.

One of the big advantages with the $k - \varepsilon$ model is that it is insensitive to values that are required to be assumed in the free stream. On the other hand the $k - \varepsilon$ model is often inaccurate where sudden acceleration of the flow occurs, and at low Reynolds number regions. The $k - \varepsilon$ model also requires wall functions, which is used to simulate the flow close to walls.

In the near wall region, where low Reynolds numbers occur, the $k - \omega$ model can be used without the requirement of wall function. However, since it does not use wall functions the mesh closest to the wall needs to be very fine.

The $k - \varepsilon$ and $k - \omega$ models have their limitations and therefore a mixture of these two models, called the $k - \omega$ SST (Shear Stress Transport) model was suggested by Menter [9]. By using a mixture of the two models the advantages of both can be used. The near wall region is modelled by the $k - \omega$ model, which makes it possible to avoid wall function, and far away from the wall the turbulence is modelled with the $k - \varepsilon$ model, to use its capability in the free stream. This is achieved by converting the $k - \varepsilon$ model to $k - \omega$ model formulation. The $k - \omega$ SST model is very similar to the standard $k - \omega$ model, but a few refinements have been made. Changes have been made to the ω equation to implement a damped cross-diffusion derivative term as well as modifying the turbulent viscosity to account for the transport of turbulent shear stress. The modelling constants are also different from the standard $k - \omega$ model. Two versions of the models, the standard $k - \omega$ model and the transformed $k - \varepsilon$ model, are connected by multiplying them with a blending function, after which the models are added together. The blending function can either be equal to one or zero. In the near wall region the blending function is equal to one and the standard $k - \omega$ model is activated. In the free stream the blending function is equal to zero and the transformed $k - \varepsilon$ model is activated. These changes to the standard model make the $k - \omega$ SST model more accurate and reliable for wider range of flows. The disadvantage of this model is that it over-predicts turbulence in regions where large normal strain can be found, for example in stagnation regions [1, 10].

The equations for the $k - \omega$ SST models are

$$\frac{\partial(\rho k)}{\partial t} + \frac{\partial(\rho U_j k)}{\partial x_j} = P - \beta^* \rho \omega k + \frac{\partial}{\partial x_j}\left[(\mu + \sigma_k \mu_t)\frac{\partial k}{\partial x_j}\right] \quad (2.6)$$

$$\frac{\partial(\rho \omega)}{\partial t} + \frac{\partial(\rho U_j \omega)}{\partial x_j} = \frac{\gamma}{\nu_t}P - \beta \rho \omega^2 + \frac{\partial}{\partial x_j}\left[(\mu + \sigma_\omega \mu_t)\frac{\partial \omega}{\partial x_j}\right] + 2(1 - F_1)\frac{\rho \sigma_{\omega 2}}{\omega}\frac{\partial k}{\partial x_j}\frac{\partial \omega}{\partial x_j} \quad (2.7)$$

where turbulent eddy viscosity μ_t is computed from

$$\mu_t = \frac{\rho a_1 k}{max(a_1 \omega, \Omega F_2)}. \quad (2.8)$$

F_1 and F_2 are a blend factors that represent inner and outer constants, respectively, which are blended as according to

$$\phi_3 = F_1 \phi_1 + (1 - F_1)\phi_2$$
$$\phi_4 = F_2 \phi_2 + (1 - F_2)\phi_1 \quad (2.9)$$

where ϕ_1 and ϕ_2 are constants [9]. When solving the $k - \omega$ SST model the exact definition of equations and constants can vary between different software package. For the definition in Fluent and CFX see [2].

2.1.2.2   Dimensionless wall distance

y^+ is a dimensionless variable that defines the first cell distance from wall related to flow velocity at the wall. y^+ is defined as

$$y^+ = \frac{y}{l_*} = \frac{y u_*}{\nu} \quad (2.10)$$

where u_* is the wall friction velocity, y is the distance to the nearest wall and l_* is a characteristic wall length, which determines the flow domain close to the wall where the flow is significantly dominated by viscosity.

y^+ is important for turbulent flows since the magnitude of inertial and viscous forces change rapidly in the near wall region. Two different approaches are available, one is using wall function for the viscosity affected region close to the wall and the other modifies the turbulence models to be able to resolve the near wall region. The maximum acceptable value for y^+ depends on how the wall interaction is modelled; different turbulence models require different maximum values. Thus the y^+ value can be used to check if the requirements for the model chosen are fulfilled [1].

2.2 Multiphase flow

Multiphase flow refers to a flow consisting of more than one phase, for example solid particles suspended in a liquid. Most of the flows found in nature are multiphase. This is also the case in many industrial applications and multiphase flow can for example be found in fluidised beds, stirred vessels and bubble columns.

A multiphase flow can be classified into two different main types; separated flow, where the two phases only have a low number of interfaces, and dispersed flow, where the two phases have many individual interfaces [1]. Furthermore the dispersed flow can be separated into two different flow regimes: dilute and dense, where the difference is the distances between the individual intersections of the dispersed phase. If the distances are large, i.e. in the dilute flow regime, the behaviour of the dispersed phase will be governed by the forces acted on it by the continuous phase. If the distances are small, i.e. in the dense flow regime, the interactions between the different intersections of the dispersed phase also become important.

In this study the focus is on a continuous fluid phase with dilute dispersed particles. Thus this type of multiphase flow will be further explained in this section.

2.2.1 Characterising parameters

A multiphase flow is typically characterised by a few parameters. One of these parameters is the dispersed phase volume fraction defined as

$$\alpha_d = \frac{\sum_{i=1}^{N_d} V^i}{V} \tag{2.11}$$

where V^i is the volume occupied by particle i and N_d the total number of particles dispersed in the volume V [1]. According to this definition the sum of dispersed phase volume fraction, α_d, and the continuous phase volume fraction, α_c, must be equal to unity.

Another essential parameter is the response time for the particle, which is required to determine several important dimensionless parameters. The momentum response time is related to the time it takes for the particle to respond to a change in continuous phase velocity. The response time is for example used in the Stokes number, St, which is defined as a ratio of a dispersed phase response time and a continuous phase response time. The Stokes number related to particle velocity is defined as

$$St = \frac{\tau_d}{\tau_c} \tag{2.12}$$

where τ_d is the response time of the dispersed phase and τ_c is the time characteristic for the continuous phase flow. The characteristic time for the continuous phase flow with a velocity v past an obstacle with a characteristic length L, can be determined from $\tau_c = \frac{v}{L}$. This results in a Stokes number defined as

$$St = \frac{\tau_d v}{L}. \tag{2.13}$$

For a Stokes number lower than unity, which often occurs for particles with a small diameter, the dispersed phase flow is correlated with the flow of the continuous phase. This means that the dispersed phase will almost completely follow the fluid flow. For a high Stokes numbers the dispersed phase flow is uncorrelated with the continuous phase and will not follow the continuous phase flow characteristics.

The dispersed phase Reynolds number, Re_d, is another parameter that is used to characterise multiphase flow. Just as for the flow Reynolds number, (2.1), Re_d is a ratio between the inertial forces and the viscous forces. It is defined as

$$Re_d = \frac{\rho_c d_d |u - v|}{\mu_c} \tag{2.14}$$

where d_d is the diameter of the particle, u and v are the instantaneous velocities of the particle and the fluid, respectively. The density ρ_c and dynamic viscosity μ_c are the properties of the continuous phase [8].

2.2.2 Coupling between phases

When modelling two-phase flow the interaction between the phases is important. The interaction can be classified according to the level of coupling. If two phases are coupled they can exchange heat, mass and momentum. Depending on whether the dispersed phase influences the continuous phase flow and whether particle-particle interaction occurs, different simplifications in the coupling can be made.

The simplest case is called one way coupling, which assumes that the only effect that is important is the influence of the continuous phase on the dispersed phase. This implies that the effect of the dispersed phase on the continuous phase is negligible, as well as the particle-particle interactions. One way coupling is a valid assumption at a Stokes number lower than unity and at low volume fractions of the dispersed phase, i.e. when the dispersed phase has a low effect on the average density of the mixture [1].

The second level of coupling is two way coupling. The two way coupling accounts for both the influence from the continuous phase on the dispersed phase and vice versa. This is a valid assumption when the flow is still sufficiently dilute.

The third, and most advanced level of coupling, is four way coupling which, additionally to two way coupling, also accounts for the particle-particle interaction. This is applied if the volume fraction of the dispersed phase is sufficiently large, typically above 10^{-3}, and at high Stokes numbers [1].

2.2.3 Forces acting on dispersed flow

The forces acting on a particle i in a dispersed phase can be described by Newton's second law, the equation of motion,

$$m_d \frac{du_i}{dt} = \sum_j F_{i,f} \qquad (2.15)$$

where m_d is the mass of the particle, u_i the velocity of the particle and $F_{i,f}$ represents all the possible forces f that are acting on the dispersed particle [1]. The forces can be separated into two main categories: body forces and surface forces due to motion. Controversy exists in how to define these different forces. Examples on how to express them, together with a brief discussion on when they are important to include in the equation of motion, is found in this section [1, 6].

The most obvious body force is gravity, which is almost always included in the equation of motion. Other body forces that can be relevant are the Coulomb force, that arises from differences in the charge on a particle and the local electromagnetic field, and thermophoretic forces, that arise due to the temperature gradient in the continuous phase surrounding a particle [6].

The drag force is a force that acts on a particle in a velocity field when there is no acceleration on the relative velocity. The drag force for a particle i is quantified through the following equation

$$F_{i,f} = \frac{1}{2} A_d C_D \rho_d |v - u|(v - u) \qquad (2.16)$$

where A_d is the projected area of the particle normal to the flow, C_D is a drag coefficient and ρ_c is the density of the continuous phase. The drag coefficient C_D is a scalar for spherical particles and depends on, for example, the particle shape and the Reynolds number. The drag increases with increased turbulence and is generally lower for fluid particles than for solid particles. Different correlations exist for how to calculate the value of C_D. These correlations are typically valid in different flow regimes, which are defined according to the particle Reynolds number [6].

The pressure force P and shear force τ can be expressed in terms of their gradient over the particle.

$$F_{i,f} = V_d(-\frac{dP}{dx_i} + \frac{d\tau_{i,j}}{dx_j}) \qquad (2.17)$$

where V_d is the volume of the particle.

If a particle is rotating it induces a lifting force. This can be caused by various phenomena and therefore give rise to different lift forces. For example, Saffman lift force is due to a pressure distribution which is developed by a particle when it is present in a flow with a velocity gradient. A higher velocity on one side of the particle results in lower pressure, and vice versa. Another lift force is the Magnus lift force, where the rotation of a particle causes a pressure differential between the different sides of the particle, due to the difference in velocity caused by the rotation [6].

For spherical particles at low Reynold number, accurate models for these forces can be found, however, there is little data available for flow at high Reynolds numbers [1].

The buoyancy force for a particle arises from the pressure exerted on the particle by the continuous phase. It is expressed as

$$F_{i,f} = V_d g(u_i - v) \tag{2.18}$$

and it is equal to the weight of the fluid displaced by the particle [1].

Due to acceleration or deceleration of the particle or the surrounding fluid, a virtual, or apparent, mass arises. The name indicates that this form drag results in a force that is equivalent to the addition of a mass to the sphere, called the virtual mass force. This force is only applied to transient flows and can be neglected when the density of the particle is much higher than the one for the continuous phase, or when the virtual mass is much less than the mass of the particle [1].

The Basset force is the force that accounts for the viscous effect. It arises from the time required to develop the boundary layer around the particle when the particle is accelerated or decelerated. This leads to separation of timescales between the fluid and the particle. This force is sometimes called a history force since it depends on the acceleration history up to the present time. This force is in general difficult and computationally expensive to evaluate and is only relevant in unsteady flows [6].

The turbulence of the continuous phase causes a turbulent force on a dispersed particle. This force is usually modelled as a random addition to the fluid velocity and is referred to as turbulent dispersion. The force from the collision of the particles is also randomly modelled. This force is called a Brownian force and is modelled as a Gaussian white noise. The Brownian force is only important for submicrometer particles [1].

In steady, dilute flows, with dispersed spherical particles and $\rho_d >> \rho_c$, it is possible to consider only the gravity, drag and buoyancy force. Newton's equation of motion can then be significantly simplified and the resulting equation to solve is

$$\frac{du}{dt} = \frac{1}{\tau_d}(u_d - v) + (1 - \frac{\rho_c}{\rho_d})g. \tag{2.19}$$

2.2.4 Multiphase models

When modeling a multiphase flow a multiphase model is solved together with the governing equations. Many different models for multiphase flows are available and a few of them will be presented in this section.

In the Euler-Euler model both the phases are modelled as a continuum, which implies that the governing equations are solved for each phase. The Euler-Euler model can handle very complex systems but its result can be non-optimal due to the need

of empirical information to close the model. The Euler-Euler model is commonly seen as the general model for dispersed multiphase flow and can be used when no other models are suitable.

An alternative to the Euler-Euler model is the Euler-Lagrangian model. Over time this model has received several different names, for example discrete particle method or Lagrangian particle tracking (LPT). The last one, LPT, will be used in this study. In this model the continuous phase is modelled as a continuum while the dispersed phase is modelled as a large number of particles. This model is further discussed in Section 2.2.4.1.

Other common multiphase models are mixture models, for which the phases are assumed to interact strongly, and the Volume-of-fluid model, a type of Euler-Euler model where the interfaces between the phases are tracked.

The decision of which model to use is based on the physics in the system. Some important parameters are whether the flow is dispersed or separated, the value of Stokes number, the local volume fractions, the total number of particles and what type of coupling that is used.

2.2.4.1 Lagrangian Particle Tracking

In the LPT model particles are tracked by solving the equation of motion for a small body, commonly assumed as a point-particle, dispersed in a flow field. By assuming point-particle the particle has zero volume and does not affect the carrier flow filed which indicates that the volume fraction of the continuous phase is unity [6]. Therefore the flow field can be calculated by solving the governing equations. The motion of the particles is calculated by solving Newton's second law, (2.15), with the right hand side including all the relevant forces acting on the particle. These equations are then solved. First the instantaneous fluid velocity at the location of the particle, which is a sum of the local mean velocities, is determined. This will give the particle motion at that point. Since several Lagrangian time steps are performed within one Eulerian time step, the source term for the fluid motion is updated when the particle motion, during that Eulerian time step, is calculated [8].

For dispersed multiphase flow the LPT model is usually the most accurate model. It is more accurate than the Euler-Euler model since it contains less assumptions in its derivation [4]. The main limitation of LPT is the number of particles existing in the system, since the volume fraction is required to be low. The calculations are significantly simplified when one- or two-way coupling is used, compared to four-way coupling. Hence the computational demand for the calculations is strongly dependent on the coupling between the phases.

To reduce the computational demands when tracking a large number of particles, it is possible to employ the concept of computational parcels. This implies that identical particles can be considered as a parcel, or cloud, of particles that are moving with the same velocity. This can be a valid assumption for dilute flows,

where the frequency of particle collisions is low. This assumption is implemented for LPT in most of the available software programs used today. Further reading about the usage of parcels and the errors associated with their assumptions can be found in [4].

2.2.5 Wall interaction of the discrete phase

When modelling a multiphase flow the discrete phase's interaction with a wall needs to be defined. This interaction can be modelled in several different ways and a few of these models will be presented in this section.

2.2.5.1 Coefficient of restitution

The most simple way to model a particle interacting with a wall is by using a coefficient of restitution e (COR). The COR describes the energy loss, in normal direction, when a particle is colliding with a wall surface. It is defined as a ratio between the incoming impact velocity and outgoing resulting particle velocity, u_{imp} and u_{res} respectively, according to the following equation

$$e = -\frac{u_{res}}{u_{imp}}. \tag{2.20}$$

The COR can vary from 0 to 1, where 1 represents an elastic collision where all energy is conserved through the interaction. The COR can be globalised by using the following definition

$$\epsilon = -\frac{u_{res}}{u_{\infty}} \tag{2.21}$$

where the u_{∞} is the velocity before it decreases due to interaction with the wall. For large Stokes number the collision impact occurs at $u_{imp} \sim u_{\infty}$ and therefore $\epsilon \sim e$ [12]. The definition from (2.21) is commonly applied for COR, since it provides a description of the particle rebound without having to describe all the details in the physical mechanism involved.

Coefficient of restitution is widely used and plenty of experimental work has been performed to find correlations for it. Most correlations are valid for solid particles in gas flow, but some have a wider field of applicable phase and material combinations. One example of these correlations is presented by Legendrea et al. [12].

$$\epsilon = \epsilon_{max} \exp(-\frac{\beta}{St}) \tag{2.22}$$

where St is defined as the Stokes number for a particle away from the wall

$$St = \frac{(\rho_d + C_{M\infty}\rho_c)u_{\infty}d_d}{9\mu_c} \tag{2.23}$$

where μ_c is the viscosity of the continuous phase. $C_{M\infty}$ is a constant equal to $\frac{1}{2}$ while β is a parameter that includes the viscous effect of the film drainage, here set to $\beta = 35$. ϵ_{max} is the maximum value that can be reached for a particle, i.e. when

$St \to \infty$, and is experimentally determined to be the constant value of $\epsilon_{max} = 0.91$. This correlation can be used for a wide range of materials, for both of the phases, provided that the particle or droplet is spherical. In Legendrea et al. [12] the correlation is proven to fit the general trend from experimental data provided by available sources, which is for example data for toluene drops in water and liquid drops in air.

2.2.5.2 Wall film

When liquids are interacting with a wall there is a possibility that impinging droplets will form a liquid film on the surface which will strongly impact the characteristics of the droplet-wall interaction. A wall film model usually consists of a two dimensional, thin liquid film on a wall surface in a three dimensional domain. The modeling of a wall film is complex and different models have been suggested. One of those models, the Eulerian wall film model, which is implemented in Fluent, will be presented in this section.

Conservation equations

In the Eulerian wall film model the wall film is described by conservation equations. The conservation of mass is described by

$$\frac{\partial h}{\partial t} + \nabla_s \cdot (h\vec{V_l}) = \frac{\dot{m}_s}{\rho_l} \tag{2.24}$$

where ρ_l is the liquid density, h the film height, ∇_s the surface gradient operator, $\vec{V_l}$ the mean film velocity and $\dot{m}_s$ the mass source per unit wall area from the droplet impinge [2].

The conservation of film momentum is described by

$$\frac{\partial h\vec{V_l}}{\partial t} + \nabla_s \cdot (h\vec{V_l}\vec{V_l}) = -\frac{h\nabla_s P_L}{\rho_l} + (\vec{g_t})h + \frac{3}{2\rho_l}\vec{\tau_{fs}} - \frac{3\nu_l}{h}\vec{V_l} + \frac{\dot{q}}{\rho_l} \tag{2.25}$$

where

$$P_L = P_{gas} + P_h + P_\sigma \tag{2.26}$$

$$P_h = \rho h(\vec{n} \cdot \vec{g}) \tag{2.27}$$

$$P_\sigma = \sigma\nabla_s. \tag{2.28}$$

These two conservation equations can be complimented with a conservation energy equation if desired. The conservation equations can interact with LPT through source terms, $\dot{m}_s$ and $\dot{q}_s$, which models the collection of the discrete particle streams hitting the wall [2].

Impinge outcomes and film break up

An incoming droplet can impinge the wall film with four different outcomes. The droplet can stick, which implies that the droplet impacts the wall with little energy and remains nearly spherical, or it can spread, which implies that the droplet spreads out into the liquid film. The droplet can also splash, which implies that part of the impinging drop is joining the film and part of the drop is leaving the wall in the form of several smaller droplets. The final impinge is rebound, which implies that the droplet leaves the surface with changed velocity but relatively intact.

In the Eulerian wall film model the impinge outcome is determined by the impact energy E defined as

$$E^2 = \frac{\rho_l V_r^2 d_d}{\sigma} \left(\frac{1}{min(h/d_d, 1) + \delta_{bl}/d_d} \right) \tag{2.29}$$

where σ is the surface tension of the liquid and δ_{bl} is the boundary layer thickness defined as $\delta_{bl} = \frac{d_d}{\sqrt{Re}}$. A simplified illustration of the four impinge outcomes and their relation to the droplet impact energy and liquid wall temperature T, including boiling temperature T_b, are shown in Figure 2.1. Below the liquid boiling temperature the droplet can either stick, spread or splash, while above the liquid boiling temperature it can either rebound or splash. The sticking occurs if $E \leq 16$ and the splashing if $E \geq 57.7$. If the droplet is rebounding it is described by a COR depending on the impingement angle [2].
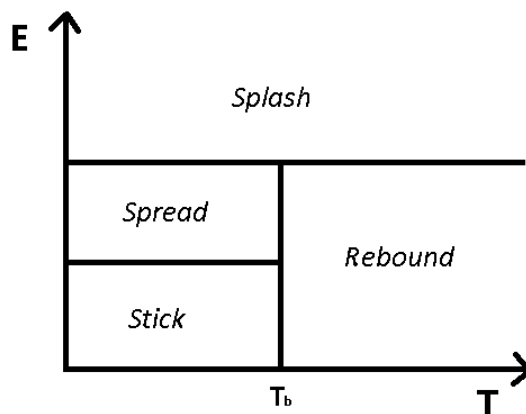
Figure 2.1: Simplified illustration of the four different types of possible wall impingement outcomes, for the Eulerian wall film model, and how they are related to impinge energy E and liquid wall temperature T.

As already mentioned, when the impinging droplet is splashing parts of the droplet will join the film and parts will create new particles. The amount of mass that splashes from the surface is described by a function for the splashed mass fraction.

The splashed mass fraction has a quartic dependence of E up to $E > 7500$. After this it will reach a constant maximum value of 0.70. The properties of the droplets leaving the surface, such as diameter, magnitude, and direction, are randomly sampled from distribution functions [2].

Once a wall film has been formed it can break up through separation or splitting. To be able to define the criterion for these break ups a definition of a Weber number for the film is needed. The Weber number is a dimensionless number used to characterise fluid's inertia compared to its surface tension. For a wall film the Weber number is defined as

$$We_f = \frac{\rho_l d_d |\vec{V_l}|^2}{\sigma}. \tag{2.30}$$

A wall film can separate at an edge if the Weber number and the angle is exceeding a critical value. Note that the Weber number is equal to the first factor in (2.29) [2].

If high relative velocities exist between the continuous phase and the liquid film, droplets can be stripped of the film. At sufficiently high shear rates a type of wave, called Kelvin-Helmholtz wave, formed on the film surface, which will grow until eventually droplets get stripped of from the surface [2].

Courant number
The Eulerian wall film model requires a transient solver and therefore a time step Δt needs to be defined. The general rule is that the time step needs to be shorter then the time it takes for the flow to transport past the cell. The time step is determined by the Courant number, CFL, according to the following relationship for a one dimensional case

$$\Delta t < CFL \frac{\Delta x}{U}. \tag{2.31}$$

The maximum Courant number allowed depends on which type of solver that is used. To assure convergence it is common to stepwise increase the maximum Courant number, and therefore indirectly the time step, until the desired value is reached [1].

2.3 Computational Fluid Dynamics

Computational Fluid Dynamics (CFD) is a section of fluid mechanics where numerical methods are used to solve and analyse fluid as well as multiphase flows. It originates in the solution of the Navier-Stoke equations which, with addition of desired models such as turbulence and multiphase models, is solved numerically over a computational grid [1].

CFD simulations have become an indispensable tool for engineers when it comes to flow analysis. It is used to provide insight of details for products and processes, for

both existing and potential future equipments, but can also be used for optimisation. In this section the steps of a typical CFD simulation will be presented. An overview of these steps is provided in Table 2.1 [1]. There are many commercial available programs for CFD simulations. The solution methods for two of these CFD programs, Fluent and CFX, will be explained.

Step	Includes
Geometry design	Define geometry and boundaries
Grid generation	Divide the geometry into small computational cells
Define models	Add models for turbulence, multiphase etc.
Set properties	Set density, viscosity etc.
Boundary and initial condition	The initial conditions, inlet and outlet conditions and conditions at the walls are set
Solve	Choose solver, iteration methods, transient or steady state flow and convergence requirements
Post processing	Analyse the results

Table 2.1: Overview of the steps performed in a typical CFD simulation.

2.3.1 Geometry design

A CFD simulation process starts with creating a two or three dimensional drawing of the geometry. This can be done in a computer-aided design program but can also be created directly in some CFD software. It is important that this geometry has a well defined location for domain boundaries, which will be further defined in Section 2.3.5. If the geometry is periodic or symmetric a simplification of the geometry can be used to reduce the computational demand. Then only parts of the original geometry will be included in the domain and the periodicity and symmetry will be modelled with boundary conditions.

2.3.2 Grid generation

Since the equations describing the flow are nonlinear the domain needs to be discretised to obtain a numerical solution. The geometry is therefore divided into computational cells to create a computational grid for the domain. It is essential that this grid, which can also be referred to as a mesh, is of good quality to get an accurate solution. The quality of the mesh is dependent on, for example, the structure of the cells, the transition between the cells and the total number of cells. Some areas, of high interest or with high gradients, might demand a finer mesh, i.e. smaller cells, compared to other areas. A finer mesh usually provides a more accurate solution, but also demands more computational effort and therefore a higher cost.

To prove the quality of a mesh, a mesh independence study can be performed. This is done by producing several different meshes where the total number of cells is varied. A specific problem is then solved for all the different meshes and their

solutions compared. Mesh independence is achieved when the variation in the results between meshes is low enough, within user specified tolerance, so that the results can be assumed identical. The work will then continue with the independent mesh that has the lowest number of total cells.

2.3.3   Define models

In addition to the Navier-Stokes equations several other models can be added to describe the flow. This can for example be models for the turbulence of the flow, reactions that occur or if the flow constitutes of several phases. There are a number of generally accepted models, but hundreds of others are available. It is up to the user to decide which models are appropriate, thus suitable to use, in each case.

2.3.4   Set properties

To be able to solve the desired models, physical properties for the fluid and the fluid material must be specified. This can for example be material, density, viscosity etc. but which exact properties are required to be defined vary on which models are used. Many CFD software have a built in material library, where most of these properties can be found.

2.3.5   Boundary and initial conditions

The boundary and initial conditions are just as important for the solution as the equations that define the flow. The way the boundaries of a domain are defined can change the result of the model and therefore it is important to define them appropriately.

Different types of boundary conditions can be defined. Which one to use depends on the function of the boundary. For an inlet an initial velocity can be defined either in terms of mass flow or velocity. If the initial velocity is unknown the inlet can also be defined in terms of pressure. An outlet is most often defined in terms of pressure, since it results in better convergence, but it can also be defined in terms of an outflow.

Walls are defined with wall boundaries, normally with no slip as its shear condition. If no slip condition is not appropriate to use, special wall functions are needed to define the wall boundary. Other properties for the wall, such as roughness etc., can also be set. Wall boundaries can account for heat transfer and reactions at the wall, if desired.

If one part of the domain can represent the whole domain, by periodical or symmetrical translations of itself, then the domain can be simplified and only consist of that one part. The new domain will then be closed by using symmetric or periodic boundary conditions. This strongly reduces the computational demand, therefore it is very advantageous and commonly applied.

When additional models, other then the governing equations, are used they can demand additional specification at the boundaries or initial conditions. This can for example be initial turbulence intensity, for turbulence models, and definition of the injection area of the discrete phase, for multiphase models.

2.3.6 Solve

Once the problem is fully defined it is time to start the solution process. The exact way to numerically solve the governing equations, with additional models, varies between different software packages. In this section the basics of the solution methods used by CFX and Fluent will be presented. More detailed description of each solver can be found in [2].

When solving the flow a convergence criteria can be put on residual values of different components. The solution is then considered converged when this criteria is satisfied. This does not always result in a correct solution since low residuals can be reached if the initial guesses for the components are badly selected. Therefore it is often recommended to monitor other parameters, such as mass imbalance, lift and drag or other properties, and observe if there is much oscillation in their values. If these parameters oscillate much the solution can not be defined as converged and incorrect solution has been reached. A converged solution is in general found when the residuals are low and the monitors have reached a stable value [1].

2.3.6.1 CFX

CFX uses an element-based finite volume method to solve the governing equations. The domain is discretised by using a computational mesh. This computational mesh is used to construct finite volumes that conserve values for, for example, mass and momentum. Figure 2.2 (a) presents the definition of a node-centered control volume, which is used in CFX. When solving in CFX the grid has to be three dimensional, but a two dimensional figure is used to simplify the illustration. A node-centered control volume stores the fluid properties and solution variables at the grids nodes. In the figure the shaded area represents the control volume which is constructed around each node of the mesh by joining the centers of the edges and element centers surrounding the node [2].

By using finite volume method the governing equations are described with volume and surface integrals. Those integrals are discretised and will form a linearised set of discrete conservation equations. The equations are then solved with a coupled solver, which solves the equations as a single system, and with a fully implicit discretisation, which uses both the current and the later state of the system. Using a coupled solver reduces the number of iterations needed for convergence [2].

Discrete methods are based on series expansion approximation of a continuous function, for example Taylor series. The accuracy is directly related to the order of the approximation. Higher order makes the error reduce faster, but unfortunately it also makes the solver more numerically unstable. CFX uses a second order accuracy [2].
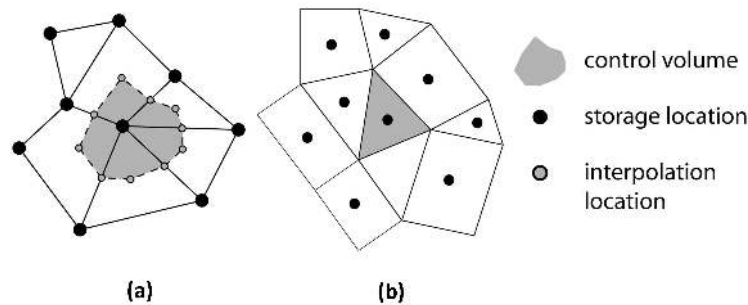
Figure 2.2: Definition of a two different control volumes. (a) presents a node-centered control volume, which is used in CFX, and (b) presents a cell-centered control volume, which is used in Fluent [7].

2.3.6.2 Fluent

As for CFX, Fluent uses a finite-volume method as discretisation scheme but, in contrast to CFX, Fluent stores discrete values at the cell centers. A cell-centered control volume can be seen in Figure 2.2 (b). Due to this storage location an interpolation value and a face value are needed, which are calculated from the cell center values, when convection terms have to be used. This interpolation is done by using upwind schemes, where the face value is derived from quantities in the cell upstream relative to the direction of the normal velocity. Several upwind schemes are available and they define the order of accuracy [2].

Since Fluent uses finite volume method the governing equations are defined as a linearised set of discrete conservation equations, as explained for CFX. Fluent offers two numerical methods to solve these equations: a pressure-based and a density-based solver. In the pressure-based solver the pressure field is obtained by manipulation of the continuity and momentum equations and solving for pressure. This method can either use coupled solver, as for CFX, or segregated solver, where equations are solved sequentially. In the density-based solver the density field is obtained from the continuity equation while the pressure field is obtained from the equation of state. This method can only use a coupled solver. In both solvers the momentum equation is used to obtain the velocity field [2].

2.3.7 Post processing

When the problem has been solved it is essential to analyse the results and the quality of the solution. To check the quality of the solution a grid independence study is usually performed, as described in Section 2.3.2, as well as evaluating the y^+ value at domain walls, as described in Section 2.1.2.2, and the convergence criterion, as described in Section 2.3.6. Once the quality of the solution is assured the results can be analysed.

3

Approach

In this chapter the approach of the study is presented. The focus will be on the main study, which is referred to as the Base case. The aim of the Base case is to get an accurate solution with as simple simulations as possible, according to requests from OneSubsea. This is done by solving a steady state multiphase flow, in a simplified geometry, using one way coupling between the phases and COR to model the droplet-wall interaction. In this section the different steps implemented to perform the Base case are described in detail. This is followed by several smaller, additional studies, that evolved from the analysis of the results of the Base case. These studies will also be explained in the end of this chapter.

3.1 Geometry design

The wet gas compressor modelled in this study is a counter rotating axial compressor consisting of an inlet, 21 compressor steps with 9 blades each, and an outlet. The general design of the compressor steps is presented in Figure 3.1.

An extremely simplified, yet representative, version of the gas compressor is used for the geometry. This is according to the request from OneSubsea. The geometry consists of one compressor blade of the initial blade passage in the compressor. The blade is stationary, thus to be able to model the rotation of a compressor step the flow has an incoming angle defined by the stagger angle of the blade and the angle of attack for the flow. The stagger angle is defined as the angle between the blade reference line and the axial direction of the compressor. The angle of attack is defined as the angle between the blade reference line and the oncoming flow.

The blade is two dimensional and its design represents the cross section at the center of a blade. This cross section is marked by a green line in Figure 3.1. The exact design of the blade is provided by OneSubsea. The axial compressor direction is set to be the horizontal direction in the geometry, hence the blade in the geometry is represented as if it has been rotated 90° from what is presented in Figure 3.1.

The geometry is created in the software program ANSA. A two dimensional domain is created, around the provided blade design, which is aligned with the stagger angle of the blade. This domain is then complemented with an inlet and an outlet situated parallel with the horizontal direction. This results in a domain with five different

boundaries: an inlet, an outlet, a blade and upper and lower sides. This domain is presented in Figure 3.2. Note the definition of the coordinate frame. This is the coordinate frame used throughout this project.
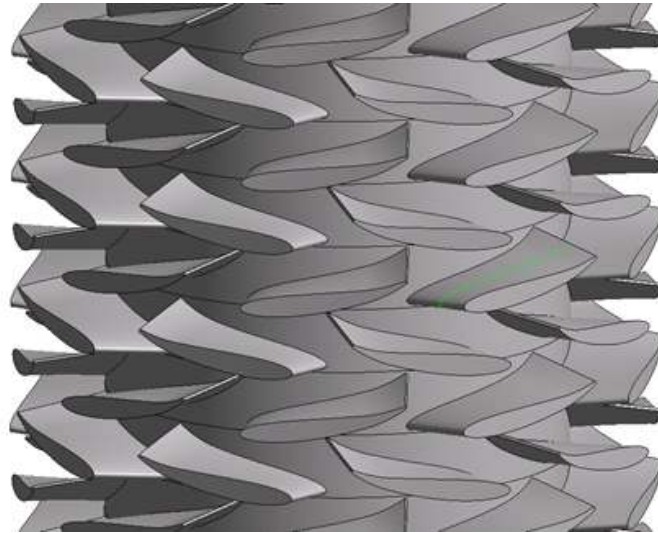
Figure 3.1: Illustration of 8 of the 21 compressor steps in the counter rotating compressor. The green line, found at a compressor blade slightly to the center-right in the figure, represents the cross sectional area on which the geometrical design of the blade is based.
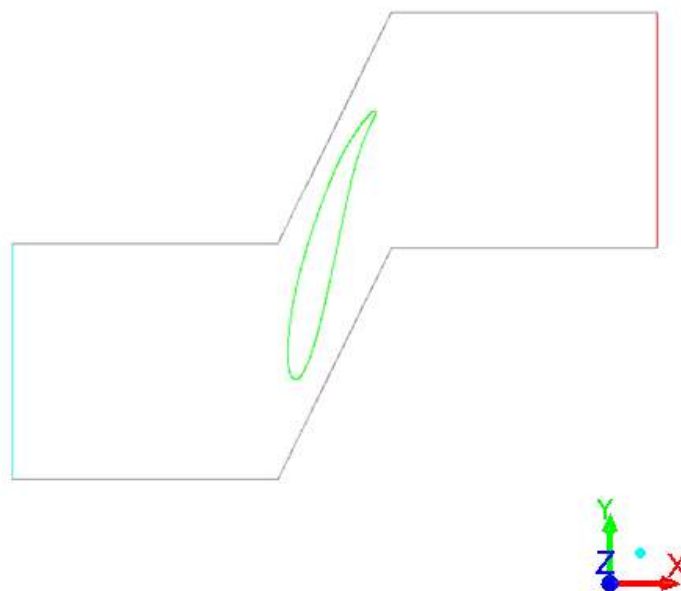
Figure 3.2: The domain with defined boundaries, colored according to: inlet - blue, outlet - red, blade - green, upper and lower sides- grey. The definition of the coordinate frame, used throughout this project, is also presented in the figure.

The exact measurements for the domain are based on the measurements of the blade and are defined through the pitch to chord ratio. This information can not be published. Therefore none of the figures illustrating the domain will present the exact design and proportions of it. The length of the domain is around 25 cm, to provide the reader an idea of the order of size for the domain.

3.2   Grid generation

The computational domain is constructed based on the geometric domain. This is also done in ANSA. The domain is meshed with quadrilateral cells and the size of the cell is adopted to the level of interest for the specific area. The smallest cells are found along the blade where the first cell has a height of 0.17 μm. The nodes on the upper and lower sides are perfectly matched to prepare for periodic boundaries, which is desired. The general look of the mesh is presented in Figure 3.3.
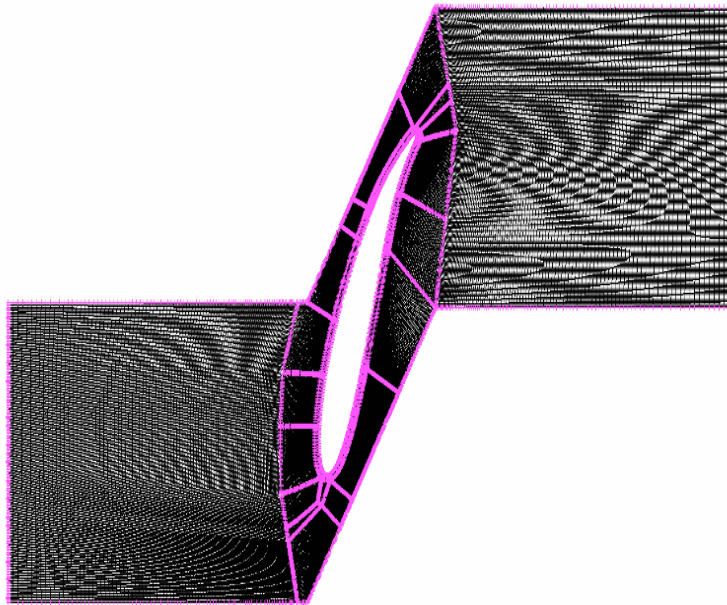
Figure 3.3: The mesh for the domain, consisting of around 178 000 quadrilateral cells with adapted cell size close the blade.

When simulating in CFX the program requires the domain to be in three dimensions. Since the domain is in two dimensions a one cell thickness in the z-direction is added to compensate this. Also, to fulfill the requirements for y^+ in CFX, some additional nodes are added close to the blade.

3.3 Define models

The equations used to model the flow are the governing equations for momentum and mass conservation. The flow is considered to be isothermal, thus the energy conservation is not modelled. The exact equations that are solved in each program can be found in [2].

3.3.1 Turbulence model

Due to high Reynolds number a turbulence model is used. For modeling the turbulence in the system the $k - \omega$ SST model is chosen. This model is suitable since it can accurately model both the droplet-wall interaction as well as the free stream flow, and it is the main model used for this type of application.

3.3.2 Multiphase model

For the multiphase modeling the LPT is chosen. This is due to its superior accuracy for this case, compared to the other models available. The forces that are included in the Newton equation of motion are gravity, drag and buoyancy. A turbulence force is modelled as well by using turbulent dispersion.

3.4 Set properties

The properties of the flow and the flow material are defined according to information provided by OneSubsea. These values are found in Table 3.1.

Parameter	Value
Material	Natural gas
Density	32.167 kg/m^3
Temperature	60°C
Angle of Attack	10°

Table 3.1: The properties of the gas flow and the flow material.

3.5 Boundary and initial conditions

The domain consists of several intersections and therefore several boundary conditions are defined. This includes boundary conditions at inlet, outlet, blade, upper and lower sides of the domain. The one cell layer thickness, i.e. three dimensional, domain used in CFX requires additional boundary conditions to enclose. The injection for the discrete phase is also defined. The initial conditions for the gas flow is presented in Table 3.2 and the calculations of the values are found in Appendix A, Section A.1.

Parameter	Value
Pressure	50 *bar*
Velocity	79.85 *m/s*
Re	2.08e07

Table 3.2: The initial conditions for the gas flow.

3.5.1   Discrete phase

The properties of the discrete phase are defined according to information provided by OneSubsea. The discrete phase is assumed to be spherical oil droplets and therefore the diameter of the droplets is used to characterize the droplet size. An assumption of one way coupling between the phases is used.

The droplets are injected from the inlet boundary and are assumed to have the same initial flow properties, such as velocity components, as the continuous phase. The droplet flow rate is varying with droplet volume fraction, therefore two different values are presented. The characteristics for the discrete phase are found in Table 3.3. Calculations for these values are presented in Appendix A, Section A.1.

Parameter	Value
Injection location	Inlet
Velocity x	12.34 *m/s*
Velocity y	78.89 *m/s*
Particle diameter	1-200 µ*m*
Flow rate	
1% Droplet volume fraction	1.52e-03 *kg/s*
2% Droplet volume fraction	3.06e-03 *kg/s*

Table 3.3: Properties of the discrete phase.

3.5.2   Inlet

The inlet is defined as a velocity inlet and therefore the initial velocity magnitude and direction and the gauge pressure is specified. The values of these parameters are found in Table 3.4. Calculations for these values are presented in Appendix A, Section A.1.

Parameter	Value
Type	Velocity inlet
Velocity x	12.34 *m/s*
Velocity y	78.89 *m/s*
Gauge Pressure	0 *Pa*

Table 3.4: Properties at the inlet boundary.

3.5.3 Outlet

The outlet is defined as a pressure outlet and therefore the gauge pressure is specified. The values of these parameters are found in Table 3.5. Calculations for these values are presented in Appendix A, Section A.1.

Parameter	Value
Type	Pressure outlet
Gauge Pressure	0 Pa

Table 3.5: Properties at the outlet boundary.

3.5.4 Blade

The blade is defined as a stationary wall with no slip condition and no wall roughness. The droplet-wall interaction is described by a constant value of a tangential and normal COR. The tangential COR is almost always equal to one and is therefore set to that value [2]. The normal COR is determined according to the method by Legendrea et al. [12], which is presented in Section 2.2.5.1. The value for the normal COR is varying with droplet size, therefore three different values are presented for three different ranges of the droplet diameter. The calculations for the COR are found in Appendix A, Section A.2, and the values for the parameters are found in Table 3.6.

Parameter	Value
Type	Wall
Shear Condition	No slip
Tangential COR	1
Normal COR	
1 μm	0.85
5, 10 μm	0.90
20, 30,..., 200 μm	0.91

Table 3.6: Properties of the blade.

3.5.5 Remaining intersections

The upper and lower sides are defined as periodic boundaries to be able to represent the complete blade row with a single blade. The one cell layer thick domain, used in CFX, is enclosed with symmetry boundaries.

3.6 Solve

The models are solved using the two software packages CFX and Fluent. In this section the solution process and the settings used for each program are presented.

For both CFX and Fluent the solution process starts with a steady state flow solution of the continuous flow, by solving the governing equations together with the $k - \omega$ SST model. When this solution converges the flow is frozen. The particles are then injected into the domain and their particle tracks are solved, using LPT, on the frozen continuous flow field.

To conclude convergence of the solution the residuals are observed. In Appendix B the graphs of the residuals from the solution process are presented.

3.6.1   CFX

Most of the solver settings used in CFX are the default. The advection scheme selected is the high resolution scheme which does not introduce as much discretisation errors as the first order schemes, but on the other hand this scheme is not as robust.

For the turbulence a first order scheme is chosen. This scheme uses an upwind advection, which is robust but introduces diffusive discretisation errors, and a first order backward Euler transient scheme, which is an implicit time step scheme that is analogous to the upwind advection scheme. The convergence criteria is selected as RMS residual type with a low target and a high number of maximum iterations, to be able to conclude from other variables if the solution converges. Mass imbalance, drag and lift are monitored to conclude if the solution converges and at the time of convergence the solver is interrupted.

3.6.2   Fluent

Most of the solver settings used in Fluent are the default. The coupled pressure-velocity scheme is chosen. This scheme provides the user with a robust and efficient implementation for single phase steady state flow, and is said to have a superior performance compared to the segregated solutions scheme [2].

For the spatial discretisation of the convection terms in the solution equation the following settings are used; The gradient is computed by the Least Squares Cell Based method, as default, since it is less expensive to compute compared to the other node based gradient methods available. For the flow the pressure discretisation scheme is of second order, and for the momentum the second order upwind scheme is used. For the turbulence the discretisation scheme for the turbulent kinetic energy and specific dissipation rate is both first order upwind.

3.7   Post processing

Once a converged solution is achieved the results are analysed. The quality of the solution is checked with a mesh independence study, presented in Section 4.1, and by observing the value of y^+ on the blade, according to reasoning presented in Section 2.3.7.

From the simulations the data of interest is outputted at the beginning of the next blade row, i.e. at the axial clearance. This location is illustrated in Figure 3.4. In Fluent a line is added at the location of the axial clearance to be able to output the desired data. In CFX this is not as simple since data from particle tracks can only be outputted at a boundary. Therefore the domain is shortened so the output is located at the axial clearance. This additional domain is only used in CFX for simulations of the particle tracks.

At the axial clearance the magnitude of the droplet velocity components, in x- and y-direction, are outputted for each of the different cases. From these velocity components the velocity angle of the outflow is computed. The velocity components and angle are then averaged. Note that for the continuous phase the data is outputted at the node points along the axial clearance line, i.e. the data is equally spaced along the axial clearance line. For the droplets the data is outputted at the point at the axial clearance line where the droplets cross, i.e. the data does not have to be equally spaced over the line. The average values are then compared and the results from this comparison are presented in Section 4.3.
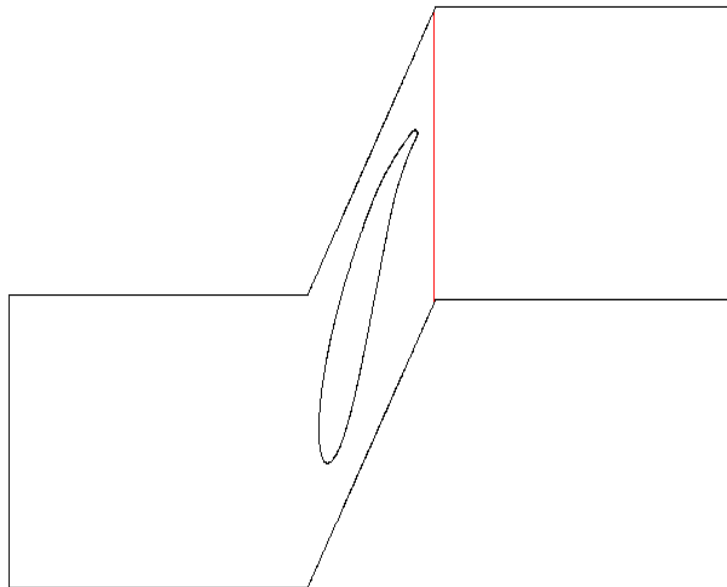
Figure 3.4: Clarification of the location of the line representing the axial clearance, where the particle data is outputted.

3.7.1 Mesh independence study

To assure that the solution is independent of the mesh, a mesh independence study is performed. The mesh presented in Section 3.2, Figure 3.3, referred to as Mesh1, is constituting of roughly 178 000 cells. Originating from Mesh1 a few different meshes are produced based on a factor for the total number of cells in the domain, excluding the near wall region where the number of nodes are kept constant. This

results in the following meshes; Mesh0.8, Mesh1.35 and Mesh1.8, where the number in the name indicates the factor used. The velocity profiles for these meshes are compared to be able to conclude mesh independence.

3.8 Additional studies

From the analysis of the results from the Base case a further evaluation of the droplet-wall interaction is done. The motivation for each one of these wall interaction studies is presented in Section 4, but the method used for them is presented in this section. Also a separate case is presented, which was set up to validate the models used in the Base case.

3.8.1 Compare case

To assure that the models used for the Base case are valid, a simulation of a validation case is performed. This case is referred to as the Compare case. It is based on a study by Tu et al. [14] where the rebound of spherical glass particles around a curved surface in flow of air is evaluated, both by experiment and CFD simulations. Several case studies are performed where the particle size, i.e. Stokes number, and flow velocity, i.e. Reynolds number, is varied. The results are presented by a normalized rebound distance, calculated by dividing the normal wall rebound distance with the curved surface diameter. Tu et al. [14] simulations show good agreement with the experimental data.

The Compare case is set up in CFX with the models used in the Base case and the domain and flow used in [14]. Three different cases with constant Reynolds number, 16 000, and three different Stokes numbers; 0.1, 4.97 and 17.6, are simulated. A comparison of the rebound distance from these cases and the Tu et al. [14] is constructed.

3.8.2 Sensitivity study of the coefficient of restitution

To evaluate the importance of the COR value a sensitivity study is performed. This is referred to as the COR study. The maximum and minimum values of the normal (N) and tangential (T) COR, i.e. 1 and 0, are simulated with four different combinations; N1 T1, N1 T0, N0 T1 and N0 T0. The COR study is performed in both Fluent and CFX. Note that in CFX a normal COR equal to 0 represents trapping the droplet at the wall. In Fluent a COR equal to 0 does not trap the droplets at the wall. Instead the droplet will rebound with a total loss of energy in that direction.

The setup and solution process for the COR study are equivalent to the Base case, except from that now the COR is varied for each particle size and that the particle tracks are only computed for four different particle sizes: 10 µm, 50 µm, 100 µm and 200 µm. The data for the droplets and their particle tracks are evaluated equivalent to the Base case.

3.8.3 Trapped case

A wall interaction study, where the droplets are trapped at the wall is performed. This is referred to as the Trapped case. This case is set up in Fluent using the same approach as the Base case, except from the boundary type at the wall which is set to trap. This means that the droplets that have collided with the wall will no longer be tracked. The data for the droplets and their particle tracks are evaluated equivalent to the Base case.

3.8.4 Wall film

A wall interaction study where the interaction is modelled by a wall film is performed. This is referred to as the Wall film. This case is set up equivalent to the Base case, except from that the droplet-wall interaction is modelled by using the Eulerian wall film model. Thus the models that are used to simulate the wall film are: the governing equations for momentum and mass conservation, the $k-\omega$ SST turbulence model, LPT and the Eulerian wall film model. As for the Base case the solution process starts with solving the governing equations together with the turbulence model. When this solution converges the continuous flow is frozen and then the Eulerian wall film model is solved transient. The settings used to solve the film is presented in Section 3.8.4.1. Once the film is solved the particle tracks are simulated.

3.8.4.1 Settings for the Eulerian wall film model

The wall film is modelled with the Eulerian wall film model, presented in Section 2.2.5.2, which is allowed to interact with the LPT. The droplets can splash, which creates four new smaller droplets, and the film is allowed to break up through stripping and separation. The momentum conservation equation includes the gravity force, the surface shear force and the pressure gradient. A maximum and minimum thickness for the film is set to 0.1 m and 1e-15 m, respectively.

The Eulerian wall film model must be solved transient and therefore a time step and a maximum value for a Courant number is defined. An adaptive time step is used to account for the difference in the mesh. The solution can easily diverge, thus the maximum Courant number is step wise increased. The solution is initiated with a time step of 1e-09 s and the maximum Courant number of 0.05, which is then increased to 0.1, 0.15 and finally kept at 0.2.

Since the Eulerian wall film model is interacting with the particle tracks, both are solved at the same time. The particle tracks are updated after every 20th wall film iteration, even though the source terms in the conservation equations for the film are updated in every iteration. The discretisation schemes used are of first order explicit for time, and first order upwind for momentum and continuity.

4

Results and Discussion

In this section the results from the CFD simulations are presented. First the results from the solution quality evaluation are presented. This is followed by a presentation of the solution for the pure gas flow. The results from the Base case are then provided, including analyse and discussion. The models used in the Base case are validated by performing the Compare case, and the results from this comparison are presented. The analysis of the Base case gave rise to several additional studies and the results from these will be presented. Finally the chapter ends with some further discussion around the results, including recommendations for future work.

The simulations were set according to the approach presented in Chapter 3. To simplify for the reader each section in this chapter will start with a brief summary of what is relevant for each case.

4.1 Solution quality

A mesh independence study was performed. No essential difference in the velocity profiles was found between the results from Mesh1, Mesh1.35 and Mesh1.8. In Figure 4.1 the difference in the velocity profiles for Mesh1 and Mesh1.8 is presented. Some difference in the velocity profiles were found between the results from Mesh0.8 and the three other meshes. Mesh1 was considered to be mesh independent thus concluded to be suitable for use in this study, for both CFX and Fluent.

The y^+ values for the Base case were observed. y^+ should be less than 2 for the $k-\omega$ SST model to be valid, according to [2]. A contour plot for how the y^+ value vary along the blade, from simulations in CFX, is presented in Figure 4.2. The maximum value of 1.24 validates the use of the $k-\omega$ SST model. The equivalent maximum value for y^+ from the simulations in Fluent was 1.19.
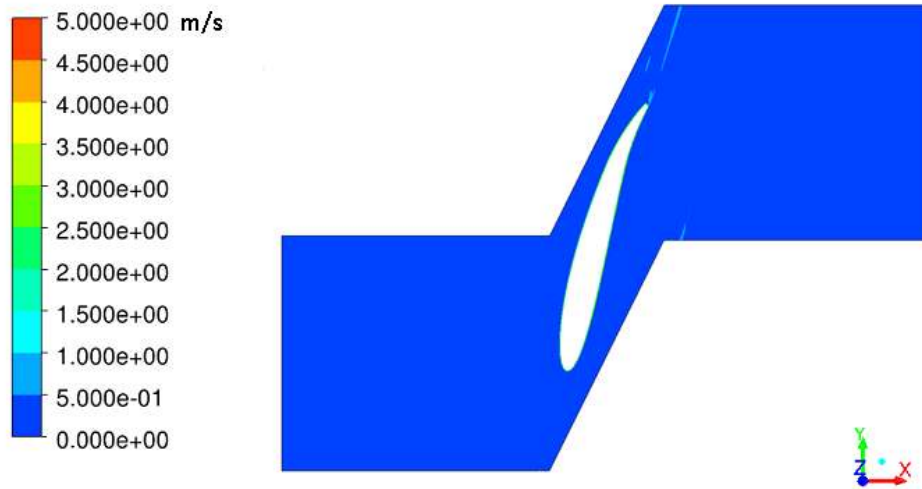
Figure 4.1: Contour plot of the difference in velocity profiles for Mesh1 and Mesh1.8, for simulations performed in Fluent. The difference is considered to be insignificant.
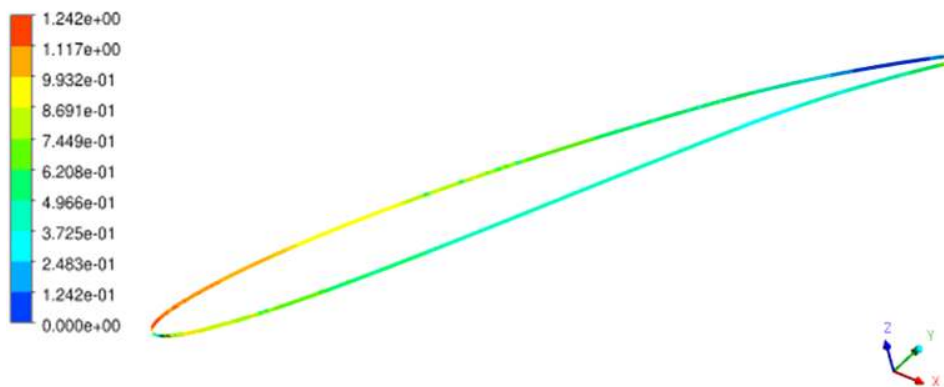
Figure 4.2: Contour of the y^+ value for simulations of the Base Case in CFX. The maximum value is 1.24.

4.2 Gas flow

Numerical simulations were performed on a natural gas flow in a two dimensional computational domain consisting of one blade in the initial blade passage of the compressor. The domain was enclosed with a velocity inlet, a pressure outlet and two periodic upper and lower sides. The blade was defined as a stationary wall with no slip condition. The governing equations for mass and momentum conservation, together with the $k - \omega$ SST turbulence model, were used to model the flow.

The velocity profile for the gas flow simulated in Fluent is presented in Figure 4.3. The results for the simulations in CFX were identical to the result from Fluent and are therefore not presented here. Note that the domain is only constituting of one blade but to illustrate the periodicity in a blade row the results are presented with three blades. The velocity magnitude of the solution varies from 0 m/s to 94.6 m/s. The highest velocity area is found just above the leading edge of the blade. A low velocity area is found at the leading edge and a stagnant velocity area is found around the trailing edge. The general look of the velocity profile is as expected.
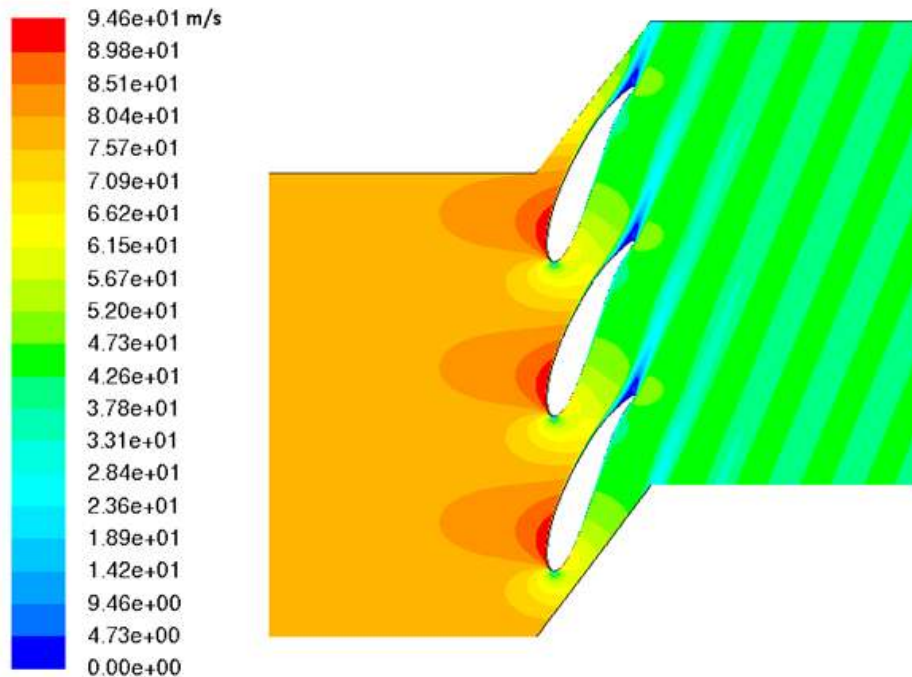
Figure 4.3: Contours of the velocity magnitude for the gas flow. The maximum velocity is found just above the leading edge and the lowest velocity is found in the stagnant area after the trailing edge.

4.3 Base case

In the Base case the particle tracks for oil droplets were solved on the frozen natural gas flow using LPT. In total 22 different case studies were performed where the droplet size was kept constant at one value within the defined size range, i.e. droplet diameter of 1-200 µm, for each case but varied between phases. One way coupling was used between the two phases and the droplet-wall interaction was modelled by using normal and tangential COR. Since one way coupling was applied for the simulations the results are independent of droplet volume fraction. Data is presented from the 1% droplet volume fraction simulations, but the results are identical for the 2% droplet volume fraction simulations. The exception is in Figure 4.8, where the results for both volume fractions are presented, even though the data is based on the 1% droplet volume fraction simulations.

According to Stokes number the results are expected to show that the flow for smaller droplets will be strongly affected by the flow of the gas. As the droplet size increases, the impact from the gas flow is expected to decrease until the droplet diameter reaches a size where the droplet flow is no longer affected by the gas flow.

Figure 4.4 and Figure 4.6 present the average velocity in x- and y-direction, respectively, at the axial clearance. Data is presented for the pure natural gas (Natural gas) and droplet volume fraction of 1% from the two programs used (Fluent, CFX). Each point represents one of the 22 cases where a constant droplet size was used for the discrete phase, i.e. 1 µm, 5 µm, 10 µm, 20 µm,...,190 µm, 200 µm.

Figure 4.4: The average velocity in x-direction at the axial clearance for different droplet sizes. Data is presented for the pure natural gas (Natural gas) and for 1% volume fraction of oil droplets from the two programs used (CFX, Fluent).

In Figure 4.4 a linear trend can be observed between the averaged velocity in x-direction and droplet size. The larger the droplet, the more its velocity differs from the velocity of the continuous phase. This is as expected. At the maximum droplet size, 200 µm, the velocity is more than 9 m/s higher than the velocity for the continuous phase. It can also be observed that the droplet velocity is differentiating from the continuous phase for the small droplets, even though the magnitude of the difference is smaller. This was not expected, but has a logical explanation. The difference is caused by the difference in how the data was collected, as explained in Section 3.7. At the stagnant area, found at the trailing edge of the blade, no droplets are found for the smallest droplets. This can be seen in Figure 4.5, where the particle tracks colored by velocity magnitude for 10 µm droplets are presented. Since the average velocity of the droplets is based on data collected at the point where the droplets cross the axial clearance line, this will result in a higher average for the droplets. The velocity is the same if you compare the velocities at the same y-coordinate on the axial clearance line.
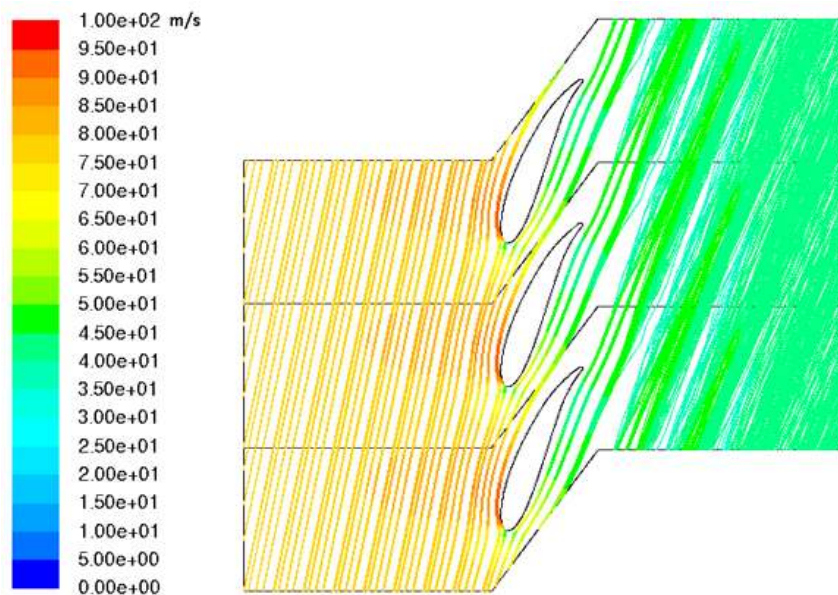
Figure 4.5: Particle tracks colored by velocity magnitude for droplets with 10 µm diameter, simulated in Fluent. Note that at the axial clearance no droplets are found at the low velocity area caused by the stagnant velocity area after the trailing edge.
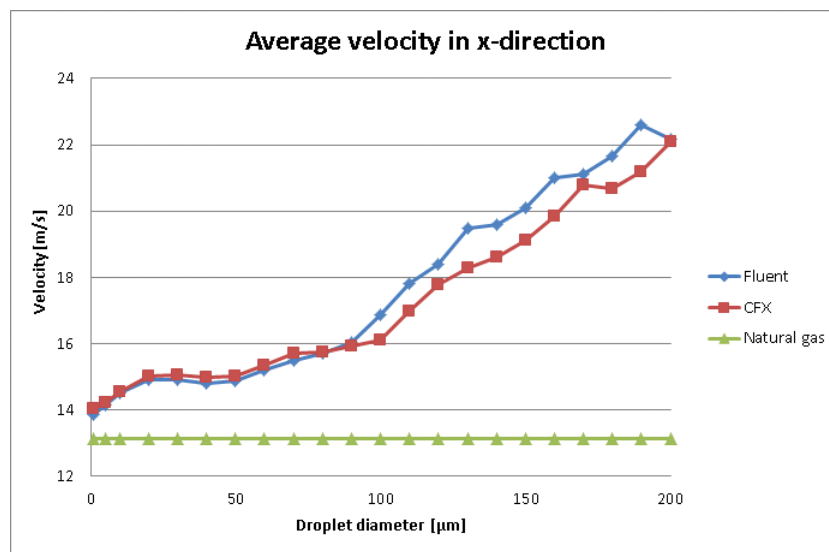

Figure 4.6: The average velocity in y-direction at the axial clearance for different droplet sizes. Data is presented for the pure natural gas (Natural gas) and for 1% volume fraction of oil droplets from the two programs used (CFX, Fluent).

It can also be observed in Figure 4.4 that there is a difference in the results for the droplet velocities for the two different programs. This is due to the differences in how the particle tracks are computed in each program, in particularly when it comes to how the programs apply the COR. This applies to the rest of the graphs provided

in this section. Further information about this can be found in the user guide's for Fluent and CFX [2].

In Figure 4.6 the average velocity in y-direction at the axial clearance for different droplet sizes is presented. The velocity for the smallest droplets differentiate from the continuous phase for the same reason as explained for the velocity in x-direction, but the rest of the trend is unalike. Initially the difference between the velocities is increasing with increased droplet size. This is followed by a turn point at 80 μm where the difference reaches a top value of 4.3 m/s for the Fluent simulations. After this the difference is decreasing with increased droplet size for the size range 90 μm - 200 μm, except for a few points around 170μm. This trend can be explained by a combined effect of how the gas flow affects the droplets and the droplets interaction with the wall. To clarify this behavior, the droplet flow has been divided into three different characteristic regions. A presentation of these regions can be found in Section 4.3.1.

In Figure 4.7 the average velocity angle at the axial clearance for different droplet sizes is presented. Initially it can be concluded that the droplets will have lower velocity angle than the continuous phase, regardless of droplet size. Two trend regimes can be observed. From 1 μm to around 70-80 μm the difference between the continuous phase and droplets is low, with a maximum difference around 1°. This trend regime represents the droplet sizes that are strongly affected by the gas flow. After 80 μm the difference is increasing relatively linearly with increased droplet size. The maximal angle difference is found at the droplet size 200 μm and is 11° and 12° in CFX and Fluent, respectively .
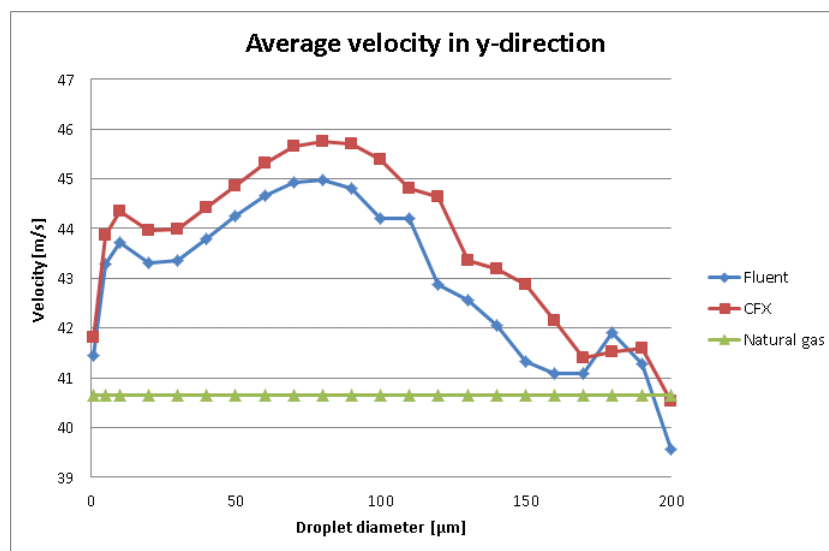

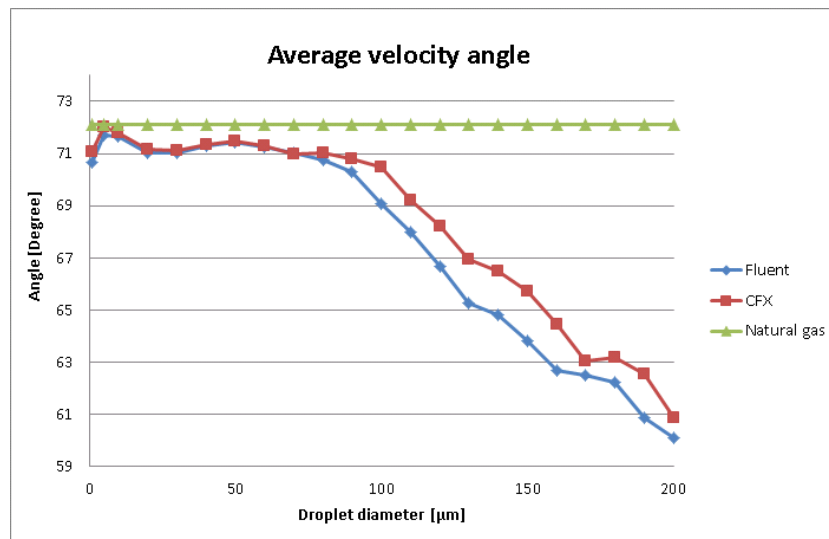**Figure 4.7:** The average velocity angle at the axial clearance for different droplet sizes. Data is presented for the pure natural gas (Natural gas) and for 1% volume fraction of oil droplets from the two programs used (CFX, Fluent).

To represent an average velocity angle for both the Natural gas and the droplet flow, a mass weighted average velocity angle (MWAVA) was calculated. It is defined as

$$MWAVA = \frac{\phi_d \dot{m}_d + \phi_c \dot{m}_c}{\dot{m}_d + \dot{m}_c} \qquad (4.1)$$

where ϕ_d and ϕ_c are the flow angle and $\dot{m}_d$ and $\dot{m}_c$ are the mass flow for the discrete and continuous phase, respectively. The calculations for MWAVA can be found in Appendix A, Section A.3, and the results from this calculations are presented in Figure 4.8. The MWAVA is presented for three different volume fractions of the droplets; pure gas, 1% and 2% of oil droplets, based on data from simulations performed Fluent.
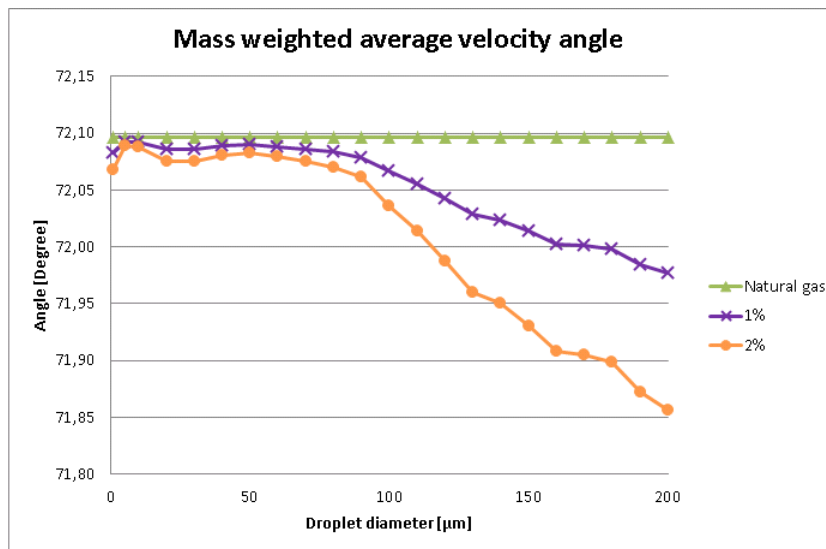
Figure 4.8: Mass weighted average velocity angle for natural gas with different volume fractions of oil droplets: pure natural gas, 1% and 2%. The data is based on simulations in Fluent.

It can be concluded that the MWAVA is decreasing with increased droplet volume fraction and increased droplet size. Figure 4.8 shows similar trend as Figure 4.7 with the two distinct trend regimes, but the magnitude for the differences is significantly lower. The difference in MWAVA remains lower than 0.05° for particles sizes up to 90 µm for 1% droplet volume fraction and 80 µm for 2% droplet volume fraction. The maximum difference in MWAVA between natural gas and oil droplets is around 0.2° and 0.35° for 1% and 2% volume fraction, respectively.

4.3.1 Characteristic flow regimes

The droplet flow has been divided into three characteristic regions to explain the trends in the velocity components. These regions are presented in this section.

4.3.1.1 Regime 1

The first flow regime, Regime 1, is characteristic for the smallest droplet sizes. In this regime the droplet flow is fully determined by the flow of the natural gas. For

these droplets the Stokes number is low. This implies that the droplets response time is much less than the time scales for the gas flow. Therefore the droplets have time to respond to changes in the gas flow. Effectively this means that the droplets will fully follow the gas flow and therefore have no significant interaction with the wall in the domain.

A typical case for Regime 1 is presented in Figure 4.9 where the particle tracks, colored by velocity magnitude, for 5 µm droplets are presented. This regime is found for droplet sizes in the approximate size range 1 µm to 20-30 µm.

Figure 4.9: Particle tracks colored by velocity magnitude for droplets with 5 µm diameter. This represents typical particle tracks in Regime 1, simulated in Fluent. Note that the droplets are following the flow around the blade and have no significant interaction with the blade.

4.3.1.2   Regime 2

The second flow regime, Regime 2, is characteristic for the relatively small droplet sizes. In this regime the droplet flow is mainly determined by the flow of the natural gas, but also affected by the interaction with the wall. The droplets are big enough to collide with the wall, but once the collision has occurred the droplets are small enough to get affected by the flow of the gas. The Stokes number is still relatively low. This implies that the droplets almost have time to respond to the difference in

velocity between the phases. Effectively this means that the droplets will have time to correct their flow pattern to the flow of the gas before crossing the axial clearance line.

A typical case for Regime 2 is presented in Figure 4.10 where the particle tracks colored by velocity magnitude for 80 µm droplets are presented. This regime is found for droplet sizes in the approximate size range 20-30 µm to 90-100 µm.
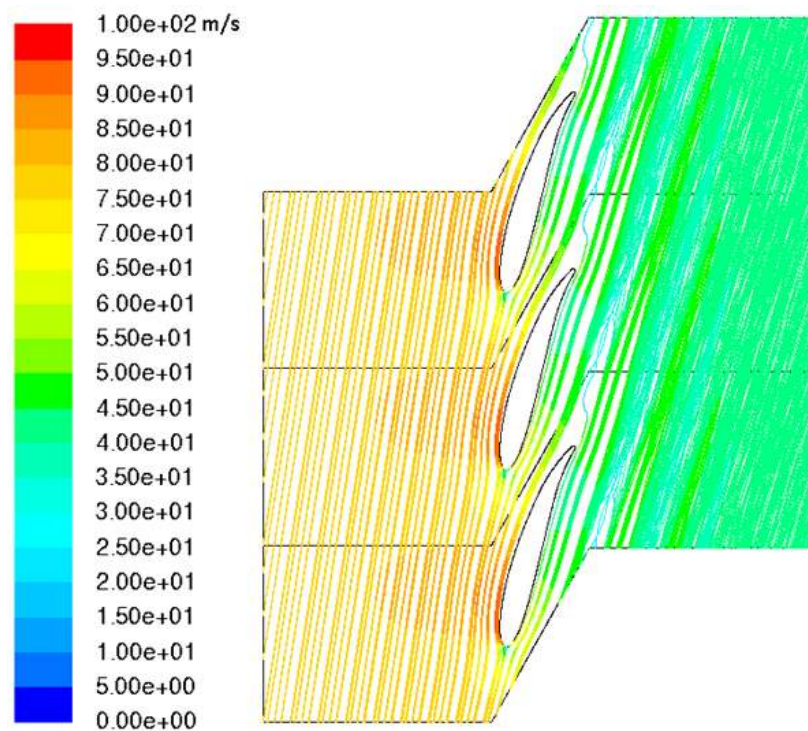

Figure 4.10: Particle tracks colored by velocity magnitude for droplets with 80 µm diameter. This represents typical particle tracks in Regime 2, simulated in Fluent. Note that the droplets are interacting with the blade and are strongly affected by the gas flow after the collision.

4.3.1.3 Regime 3

The third flow regime, Regime 3, is characteristic for the top of the droplet size range. In this regime the droplet flow is mainly determined by the interaction with the wall and the effect of the flow of natural gas is marginal. This means that the droplets will collide with the wall and the flow pattern after the collision will be decided by the collision rather then the gas flow. The Stokes number is much bigger than unity. This implies that the droplets do not have time to respond to change in the gas flow velocity. Effectively this means that the droplets will not have time to correct their flow pattern to the flow of the gas before crossing the axial clearance line.

A typical case for Regime 3 is presented in Figure 4.11 where the particle tracks colored by velocity magnitude for 170 µm droplets are presented. This regime is

found for droplet sizes in the approximate size range 90-100 µ*m* to 200 µ*m*.

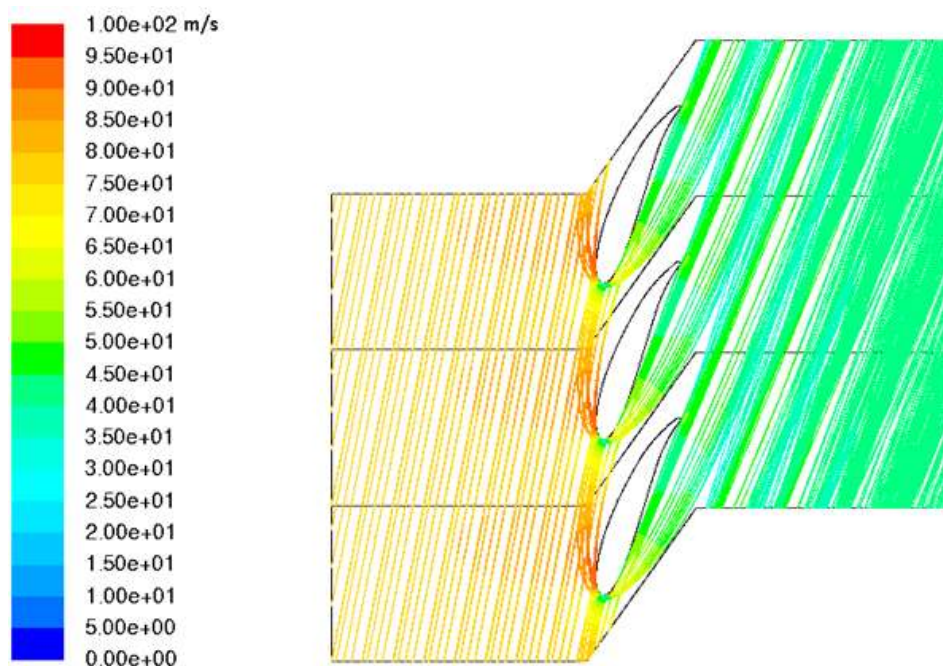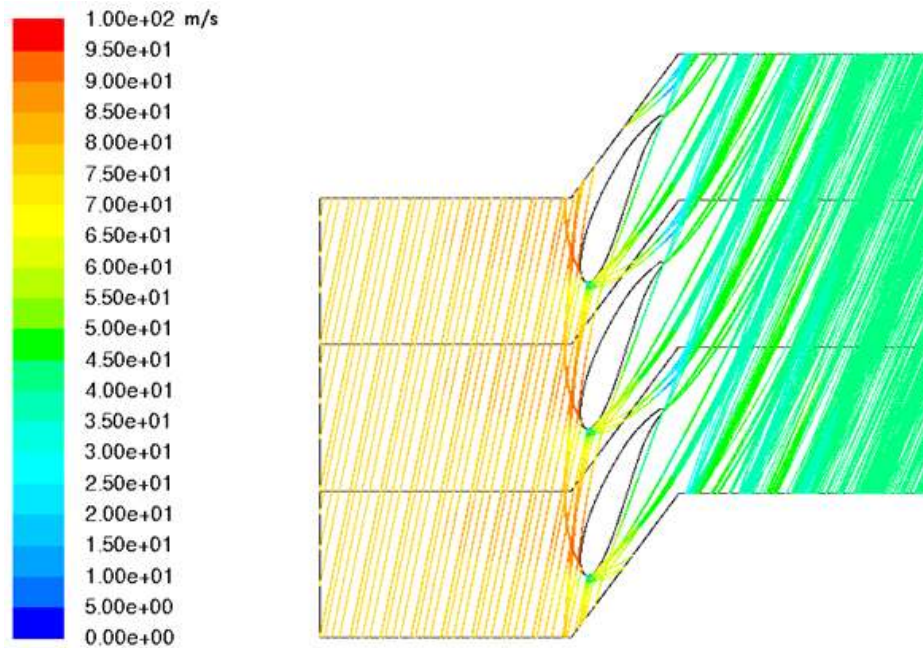**Figure 4.11:** Particle tracks colored by velocity magnitude for droplets with 170 µ*m* diameter. This represents typical particle tracks in Regime 3, simulated in Fluent. Note that the droplets are interacting with the blade and are only marginally affected by the gas flow after the collision.

4.3.2   Compare case

To validate the models used for the Base case a Compare case was set up, according to the information provided in Section 3.8.1. The result from these simulations are presented in Table 4.1 and the calculations for these values can be found in Appendix A, Section A.4. As expected the rebound distance is increasing with increased Stokes number.

Stoke number	Averaged normalized rebound distance
0.1	0
4.97	0.18
17.6	0.44

Table 4.1: Results from the calculations of the averaged normalized rebound distance for different Stokes numbers. The data is based on the simulation of the Compare case.

The results from the Compare case and the correlation with the experimental data and simulations performed by Tu et al. [14] are illustrated in Figure 4.12. It presents

the changes in normalized rebound distance with increased Stokes number. Values for the simulations performed by Tu et al. [14] are presented with the black line and their measurements from experiments are presented as black squares. The results from the Compare case simulations are represented as the red points. It can be concluded that the results from the Compare case show good agreement with the results from Tu et al. [14]. Note that in Figure 4.12 the results from the Compare case are manually included in the result graph produced by Tu et al. [14] and are therefore only providing an estimation rather than a precise location of the data from the Compare case.
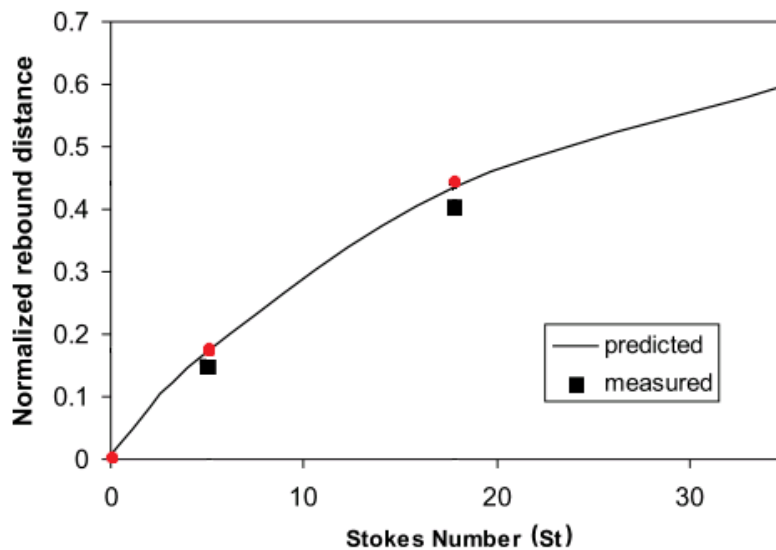
Figure 4.12: The changes in normalized rebound distance with increased Stokes number. The black line represents the results from the simulations performed by Tu et al. [14], the black squares measurements from the experiments performed by Tu et al. [14], and the red points the results from the Compare case. Note that the results from the Compare case are manually included in this graph produced by Tu et al. [14]

4.4   Wall interaction studies

When the results presented in Figure 4.4, Figure 4.6 and Figure 4.7 were analysed the importance of the droplet-wall interaction was questioned. According to the particle tracks presented in Section 4.3.1 the collisions with the wall seem to have a great impact on the droplet flow at the axial clearance line.

The potential importance of the wall interaction can be further motivated by evaluating the number of droplets that collide with the wall. The evaluation was done in Fluent by using the wall boundary type trap, which traps all droplets that collide with the wall. Therefore the number of trapped droplets is equal to the number of droplets that have collided. The result of this evaluation is presented in Figure

4.13. Here the percentage of the total number of droplets colliding with the wall, for different droplet sizes, is presented. The graph shows that already at a droplet size of 70 µm over 50% of the droplets are colliding with the wall. For the bigger droplets, from 160 µm to 200 µm, almost 90% or more of the droplets are colliding with the wall.
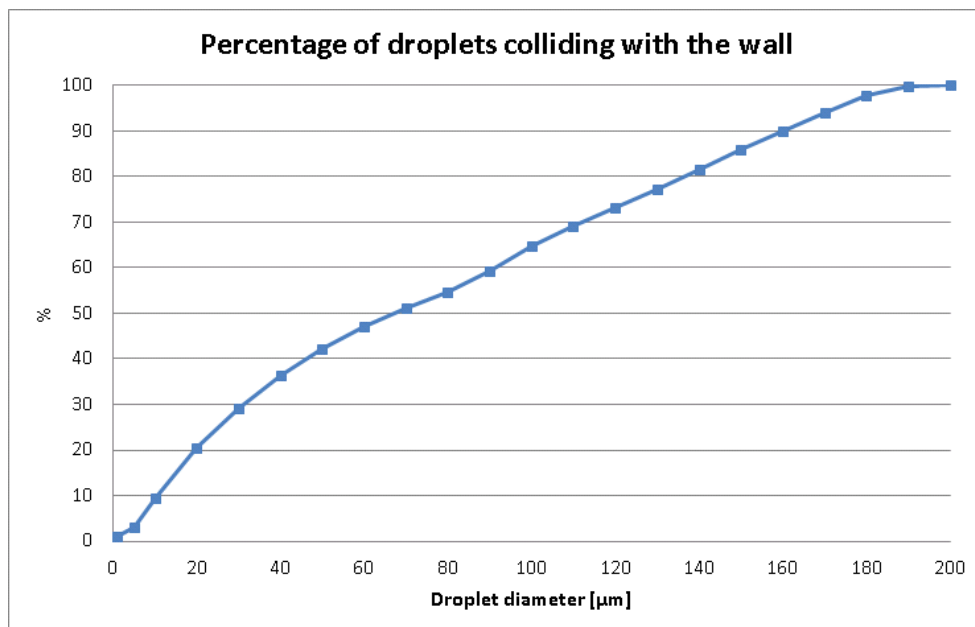
Figure 4.13: Percentage of the total number of droplets that are colliding with the blade for different droplet sizes. Note that already at a droplet size of 70 µm over 50% of the droplets are colliding with the wall.

Due to the reasons provided above a decision was made to perform further studies to evaluate the droplet-wall interaction. The results of these studies are presented in this section.

4.4.1 Sensitivity study of the coefficient of restitution

In the Base case a COR was used to model the wall interaction. There was question raised weather this is a valid model or not. The correlation by Legendrea et al. [12] is shown to have good agreement with data for liquid droplets and several studies have been found where this correlations has been used [3, 11]. The COR is a widely used, acknowledged method, but mainly applied for solid particles rather then droplets. There were also concerns raised over the high value of the COR, resulting from the correlation by Legendrea et al. [12]. The COR of around 0.9 used in the Base case is close to one, which represent an elastic collision. This is known to, in general, not be the case for colliding droplets.

To evaluate the importance of the value for the COR a sensitivity study was performed. The normal (N) and tangential (T) COR were given their maximum and minimum values, i.e. 1 and 0, and combined in the four possible combinations; N1

T1, N1 T0, N0 T1 and N0 T0. This study composed of case studies for the droplet sizes 10 µm, 50 µm, 100 µm and 200 µm with the four different combinations of COR. The results of this study are presented in Figure 4.14. Here several different graphs are provided; two (upper and lower) due to different directional components of the velocity, two (left and right) due to the different programs used, making a total of four graphs. Each graph shows the magnitude of a velocity component with the four different droplet sizes presented on the x-axis and the four different combinations of COR presented as different data series.
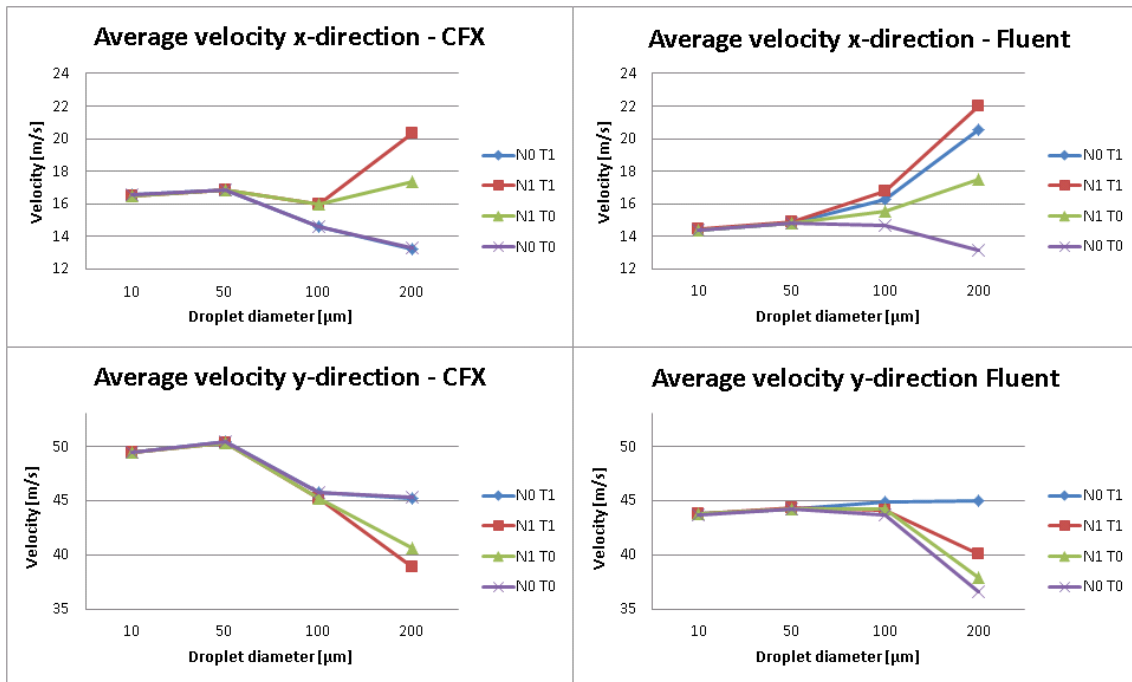
Figure 4.14: Sensitivity study of the normal (N) and tangential (T) COR. Each graph shows the magnitude of a velocity component with the case studies for four different droplet sizes presented on the x-axis and the case studies for four different combinations of COR presented as different data series. The velocity in x-direction is found at the top and the velocity in y-direction is found at the bottom. The simulation results from CFX is found on the left side and the simulation results from Fluent on the right side.

From Figure 4.14 it can be concluded that the magnitude of both the velocity components are independent of the value for COR up to 50 µm. The velocity in the y-direction is almost independent of COR for droplet sizes up to 100 µm, while at the same point the results have started to diverge for the velocity in the x-direction. For droplets bigger than 100 µm a strong divergence in the results can be seen. The biggest difference in the result for different COR is found for the velocity in the x-direction simulated in Fluent, where the difference is almost 9 m/s at 200 µm.

The conclusion from the COR study is that the magnitude of the velocity components are independent of the COR for the droplet size range 1-50 µm, almost independent for 50-100 µm and strongly dependent for 100-200 µm. These results

show strong correlation to the three characteristic flow regimes presented for the Base case.

4.4.2 Trapped case

In the Base case a COR was used to model the wall interaction. A question was raised whether or not this was a valid way to model the wall interaction for droplets. A more accurate way would be to use a wall film model. This implies that the droplets that are impinging the wall could be adsorbed to form a wall film, as described in Section 2.2.5.2, instead of just rebounding. Modelling a wall film would make the simulations significantly more advanced, which was not desired for the base case.

One alternative way to potentially model a droplet-wall film is to trap the droplets that are impinging the wall. Theoretically this could be seen as an extremely simplified model for a wall film. For the simulations of this the wall boundary type trap was used, this case is referred to as the Trapped case. The resulting velocity components for these simulations, performed in Fluent, are presented in Figure 4.15 and Figure 4.16. These graphs shows a noticeable difference compared the corresponding ones presented for the Base case, i.e. Figure 4.4 and Figure 4.6. The trend in the velocity in y-direction is the same but with different magnitude, while the velocity in x-direction is decreasing, instead of increasing, with increased droplet size.

Figure 4.15: The average velocity in x-direction for natural gas and oil droplets of different sizes, simulated in Fluent using the wall boundary type trap.

The velocity angle, presented in Figure 4.17, is also showing a significantly different trend compared to the trend for the Base case, presented in Figure 4.7. The angle is increasing, instead of decreasing, with increased droplet size. Observe that the magnitude of the increase is much lower, compared to the decrease for the Base case. The increase of the velocity angle is due to the requirement of a high velocity angle to manage to pass the blade passage without colliding with the blade, which is illustrated with a theoretical particle track in Figure 4.18. The velocity magnitude will logically be lower in the x-direction with higher velocity angle, but it will also be lower in the y-direction. This is because the velocity magnitude in total is lower

due to the low velocity area caused by the stagnant area behind the trailing edge of the blade.

Figure 4.16: The average velocity in y-direction for natural gas and oil droplets of different sizes, simulated in Fluent using the wall boundary type trap.
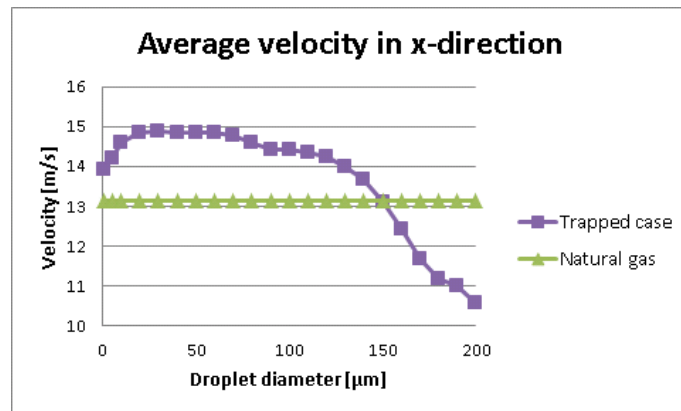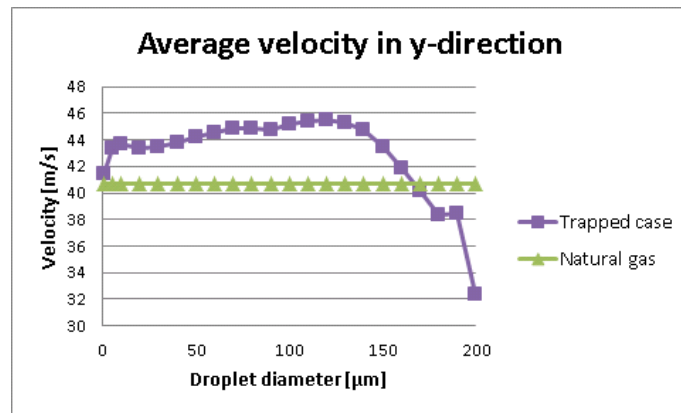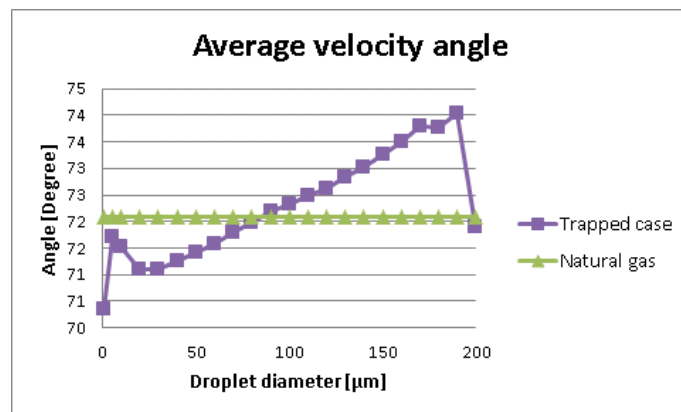

Figure 4.17: The average velocity angle for natural gas and oil droplets of different sizes, simulated in Fluent using the wall boundary type trap.
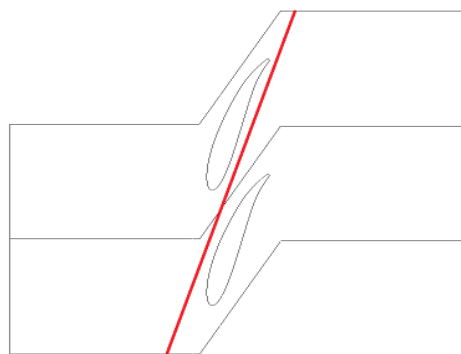

Figure 4.18: Illustration of a theoretical particle track for a droplet that passes the blade passage without colliding with the blade.

Whether these graphs provide a realistic result or not can be questioned since the data is only based on the droplets that cross the axial clearance line. These droplets correspond to a small fraction of the droplets injected into the domain, according to the results provided in Figure 4.13, and can therefore not represent the total flow. But these results can still give an idea of the characteristics of the flow. Trapping the droplets at the wall could potentially represent a extremely simplified liquid wall film, where the impingement is dominated by adsorption and splashing of the droplets, particularly if this is in combination with interest of the particle tracks rather then the characteristics of the film. The absorption is accounted for when the droplets will get trapped at the wall. The splashing is accounted for by assuming that the droplets that will splash will form droplets that are small enough to follow the flow once they have left the wall. The break up of the film can also be assumed to be modelled according to the same reasoning, i.e. the droplets that break up from the wall will be small enough to follow the flow once they have left the wall. The data for the particle tracks at the axial clearance would represent the fraction of the injected droplets that passed the blade passage without colliding with the wall. The rest of the droplets would be assumed to either be found in the wall film or perfectly following the flow.

4.4.3 Wall film

The final wall interaction study was the Wall film, which was performed by setting up a case where the wall interaction was modelled with a wall film. The Wall film was performed in Fluent using the Eulerian wall film model presented in Section 2.2.5.2. This study was done for a single droplet size: 100 µm. Unfortunately the Wall film could not be completed. This is due to the advanced level of simulations, in combination with lack of time. Instead of a qualitative result from the Wall film the results are presented to provide an idea of how the existence of a wall film can effect the flow. The main reason for the unknown quality of the results is that the Eulerian wall film model requires to be solved transient with extremely low time step, due to low maximum Courant number. Therefore the total simulation time accomplished was only 0.437 s, i.e. only fractions of what is desired, even though over 2 millions iterations were performed. Additional reason for the unknown quality of the results is that most of the model parameters were kept at default value, due to lack of time to evaluate them further.

A contour plot of the film thickness on the blade is presented in Figure 4.19. Due to the relatively low mass flow of the droplets the liquid film will be extremely thin. Even though the film is thin, its thickness is still always non zero, hence the whole blade is covered with the film. The maximum thickness is reached at the leading edge of the blade. This is as expected since most of the droplets have their primary impingement around this location. A second area with thicker film is found around the trailing edge due to both it being the end of the blade and the stagnant gas velocity zone surrounding it. The thinnest film is found on the upper side of the blade, just after the leading edge, caused by the high velocity at this location.
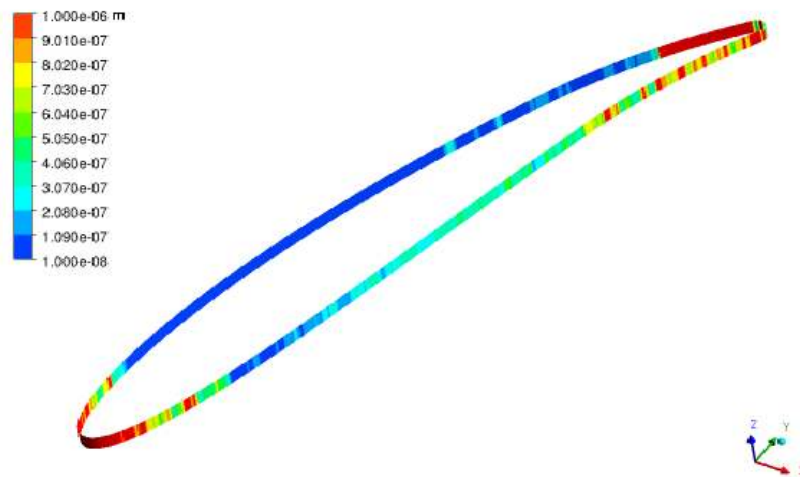
Figure 4.19: Contour plot of the thickness of the wall film on the blade.

A contour plot of the film velocity along the blade is presented in Figure 4.20. Due to thin film the velocity of the film remains low over all. High velocities are found on the leading edge of the blade, and partly at the trailing edge, i.e. the locations where the film is thick enough to prerequisite a higher velocity. As for the film thickness, even though the film velocity is low it is still always non zero.
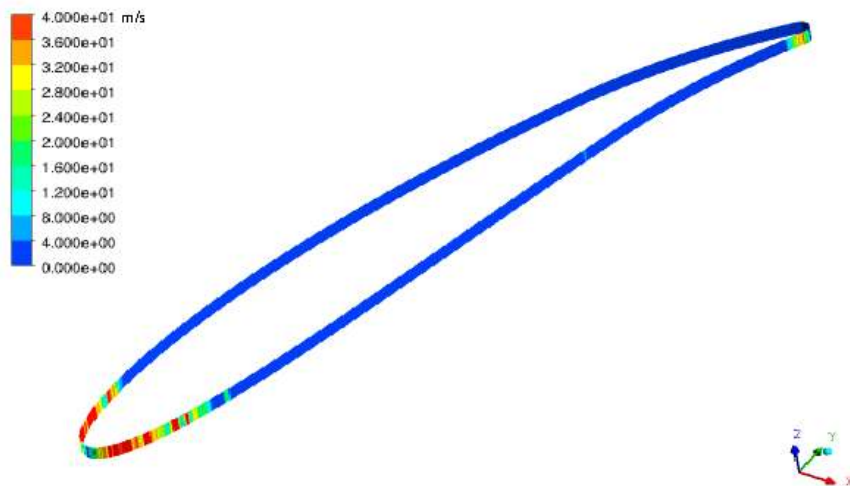
Figure 4.20: Contour plot of the velocity magnitude of the liquid in the wall film on the blade.

The Wall film simulations showed that the primary impingement outcome from droplets interacting with the wall film is splashing. This is due to the droplet's high incoming velocities. The splashing results in a significant number of smaller particles leaving the wall film. Thus the wall film simulations resulted in a non mono sized simulation, unlike the rest of the simulations in this study.

No stripping or separating of the wall film occurred. As explained in Section 2.2.5.2 stripping of the film can take place if a wave is formed at the film surface, from which droplets can be stripped. These waves could most likely not be formed due to the low thickness of the film. The separating did not occur since the domain does not contain any distinct edges.

Particle tracks from the Wall film are presented in Figure 4.21. A difference compared to the corresponding particles tracks from the Base case, which is presented in Figure B.1 in Section B.1, can be observed. The most distinct difference is that the droplets that interact with the wall in the Wall film are not rebounding off as in the Base case. Instead the droplets are splashing and forming multiple smaller droplets leaving the film. These droplets are of sizes several tenfold smaller than the original ones and are therefore strongly influenced by the gas flow. As can be seen in Figure 4.21 the splashed droplets are perfectly following the gas flow along the blade.
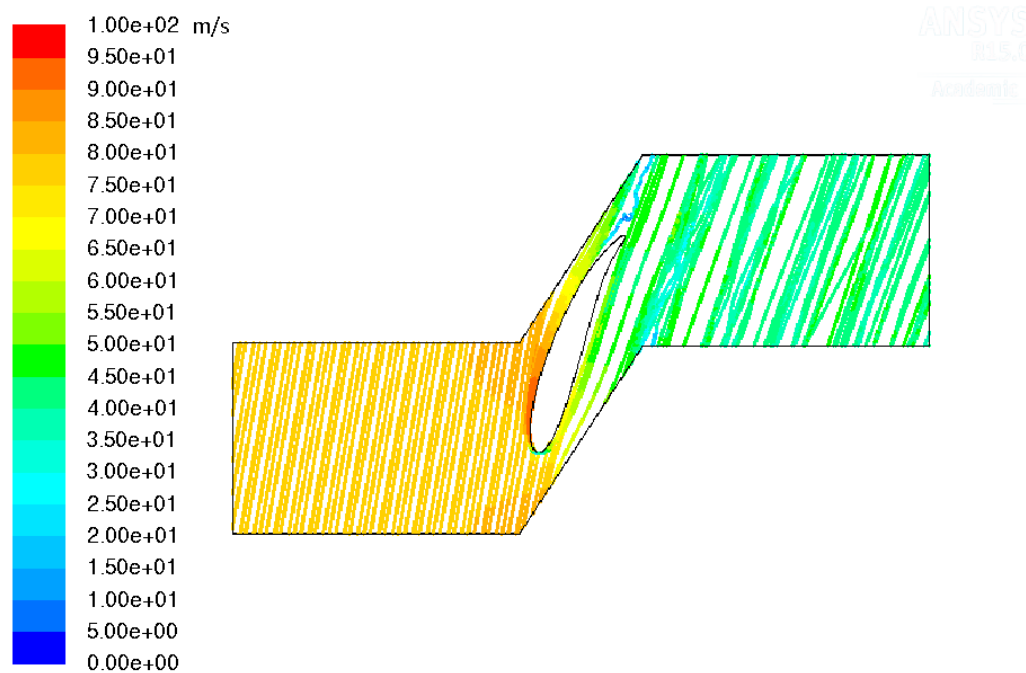
Figure 4.21: Particle tracks colored by velocity magnitude for droplets with 100 µm diameter.

The average velocity components and average velocity angle at the axial clearance for the Wall film, and the corresponding case study from the Base case, are presented in Table 4.2. When comparing these values it can be observed that the results are significantly different. This is caused by, at least partly, the way that they are calculated. The values for the Wall film are calculated using the same procedure as for the Base case, even though there is a variation in droplet size for the Wall film. To be able to truly compare these values would require that the variation in droplet size would be accounted for. The data from the Wall film has a high variation of magnitude for the velocity components, ranging from 0 to around 250 m/s. This

is, again, due to the variations in droplet size. When comparing the average magnitude for the Wall film with the Base case the velocities are lower for both the components. When comparing the average velocity angle it is slightly higher. This implies that the angle from the Wall film is closer to the average velocity angle for the continuous phase, which is as expected since the smaller droplets are following the gas flow along the blade perfectly.

Parameter	Wall film	Base case
Average velocity in x-direction	13.0 m/s	16.86 m/s
Average velocity in y-direction	40.5 m/s	44.20 m/s
Average velocity angle	71.23°	69.09°

Table 4.2: Averages values for velocity parameters at the axial clearance for a droplet injection size of 100 µm.

4.5 Further discussion

The result from the MWAVA, presented in Figure 4.8, shows relatively small affect of the droplets on the gas flow. If two way coupling had been used then the affect would have been more significant. One way coupling is, per definition, not allowing the droplets to affect the gas flow. The only possible way to represent the effect of the droplets on the gas flow is by looking at a mass flow weighed average, which most likely underestimates the effect. Since the aim of this study is to evaluate this effect it would have been more suitable to use two way coupling. Still this was not done. This is due to the request from Onesubsea to keep the simulations as simple as possible. Both since these simulations are the first ones done on the multiphase flow in their wet gas compressor, but also since they want to be able to use the results in their one dimensional modeling of the the whole process.

Another motivation for why two way simulations should be of interest for future work concerns the droplet volume fraction and Stokes number applied in this study. According to the general rules for when to apply which coupling this case should be modelled with two way coupling, since the Stokes number is larger than unity for majority of the size range, in combination with a relatively high volume fraction. Four way coupling does not need to be considered since the flow is still sufficiently dilute. Even though the two way coupling would be optimal for our case the one way coupling was found to be a good model according to the validation results from the compare case.

The domain used in this study represents the first blade row in the compressor. This implies that the flow approaching the blade is homogeneous, i.e. the droplets are evenly dispersed and have the same flow properties as the gas flow. This will not be the case after the first blade row has been passed. The differences between the gas and droplet flow will accumulate for each step, which may increase the effect of the droplets on the flow. Therefore it would be recommended to extend the domain to

include at least one or two more blade rows. Also, by including several rows in the domain, the counter rotation of the blade rows can be simulated.

As presented in Section 4.4.3 further modelling of a wall film is recommend. According to the theory this is the most accurate way of modeling the droplet wall interaction and it seems to have a great impact on the resulting particle tracks.

5

Conclusion

The results from the Base case showed that the presence of oil droplets in the gas flow will have an effect on the flow entering the next step of the compressor. The presence of droplets will reduce the velocity angle for the flow for all droplet sizes within the evaluated range. When comparing the velocity angle between the pure gas flow and the particle tracks from the droplets, the magnitude of the angle difference was found at a relatively constant value, less then 1°, for droplets smaller than 70 µm and had a maximum value of 12° at droplet diameter of 200 µm. When representing the total outflow angle with a mass weighted angle for both the gas flow and the droplets, i.e. by using MWAVA, the magnitude of the decrease is relatively small, lower than 1° for the whole droplet size range, for the low droplet volume fraction used in this study.

The Base case provides a good insight of the droplet flow around the compressor blade by observing the particle tracks. The droplet's size range could be separated into three different characteristic flow regions, according to two factors; how much the droplets are affected by the gas flow and how much the droplets are interacting with the wall.

The models used for the Base case were validated by performing a Compare case. These results were compared to the results produced by Tu et al. [14], whom used COR to model the droplet-wall interaction, and showed good agreement. Still concerns were raised whether or not this is an accurate way to model a droplet-wall interaction, which lead to further investigation.

Evaluation of the number of droplets colliding with the wall showed that already at 70 µm, over 50% of the droplets were colliding. The sensitivity study of the COR showed that the velocity angle at the axial clearance was independent of COR for droplet sizes up to 50 µm, almost independent up to 100 µm and strongly dependent for the rest of the size range. Thus it is possible to conclude that for the small droplets, definitely for droplets up to 50 µm but most likely up to around 100 µm, the result from the Base case is considered accurate.

The wall interaction in the Wall film case was modelled using the Eulerian wall film model. This case study could not be completed due to the advanced level of simulation in combination with lack of time. Instead a qualitative result of the the wall film simulations has been presented, to provide an idea of how the existence of a wall film can effect the flow. The simulations show that the primary impingement

outcome from droplets interacting with the wall film is splashing due to their high incoming velocities. This results in a significant number of small particles leaving the wall film, which, due to their small size, from that point perfectly followed the gas flow around the blade. Further work evaluating the wall film is strongly recommended.

Bibliography

[1] Andersson B, Andersson R, Håkansson L, Mortensen M, Sudiyo R, van Wachem B. Computational Fluid Dynamics for Engineers. United Kingdom: Cambridge University Press; 2012

[2] ANSYS® Academic Research, Release 15.0, Help System, ANSYS, Inc.

[3] Ardekani AM and Rangel RH.Numerical investigation of particle–particle and particle–wall collisions in a viscous fluid. J. Fluid Mech. 2008;596:437- 466. DOI: 10.1017/S0022112007009688

[4] Benyahia S, Galvin JE. Estimation of Numerical Errors Related to Some Basic Assumptions in Discrete Particle Methods. Ind. Eng. Chem. Res. 2010;49(21):10588-10605. DOI: 10.1021/ie100662z

[5] Crowe CT, Elger DF, Williams BC, Roberson JA. Engineering Fluid Mechanics. 9th ed. Asia: John Wiley & Sons; 2010

[6] Crowe CT, Schwarzkopf JD, Sommerfeld M, Tsuji Y. Multiphase Flows with Droplets and Particles, 2nd ed. USA: CRC Press;2012

[7] Fuchs R, Peikert R, Hauser H, Filip S. and Muigg P. Parallel Vectors Criteria for Unsteady Flow Vortices. TVCG 2008;14(3):615-626. DOI: 10.1109/TVCG.2007.70633

[8] Goöz MF, Sommerfeld M, Laín, S. Instabilities in Lagrangian tracking of bubbles and particles in two-phase flow. 2006;52(2):469-477. DOI: 10.1002/aic.10670

[9] Menter FR. Two-Equation Eddy-Viscosity Turbulence Models for Engineering Applications. AIAA Journal. 1994;32(8):1598-1605. DOI: 10.2514/3.12149

[10] Kumaran K and Babu V. A comparison of the numerical predictions of the supersonic combustion of Hydrogen using the S-A and SST k-ω models. Progress in Computational Fluid Dynamics. 2009;9(8):475-489. DOI: 10.1504/PCFD.2009.027765

[11] Legendrea D, Daniel C and Guiraud P. Experimental study of a drop bouncing on a wall in a liquid. Physics of Fluids. 2005;17(9). DOI: 10.1063/1.2010527

[12] Legendrea D, Zenitb R, Danielc C, Guiraud P. A note on the modelling of the bouncing of spherical drops or solid spheres on a wall in viscous fluid. Chemical Engineering Science. 2006;61(11):3543-3549. DOI 10.1016/j.ces.2005.12.028

[13] OneSubsea. OneSubseas homepage [Internet]. Norway: OnesubSea; 2015[updated 2015; cited 2015 June 1]. Available from: https://www.onesubsea.com

[14] Tu JY, Yeoh GH, Morsi YS and Yang W. A Study of Particle Rebounding Characteristics of a Gas-Particle Flow over a Curved Wall Surface. Aerosol Science and Technology. 2004;38:739-755. DOI:10.1080/02786820490490128

[15] White FM. Fluid Mechanics. 7th ed. New York: McGraw-Hill; 2008

A

Calculations

In this chapter complement calculations for the initial parameters are provided. Also the approach and results for the MWAVA calculations, and an explanation for the calculations for the Compare case, are presented.

A.1 Flow properties

Here the calculations of the flow properties will be presented in more detail. First the properties of the continuous phase, i.e. the natural gas, will be presented. This will be followed by the properties of the discrete phase, i.e. the oil droplets.

A.1.1 Natural gas

In Table A.1 the parameters used for the flow of natural gas is presented.

Variable	Symbol	Value
Pressure*	P	50 bar
Temperature*	T	333 K
Rotational speed*	ω_{RPM}	4500 RPM
Density*	ρ_c	32.167 kg/m^2
Viscosity*	μ_c	1.24e-05 $kg/(m \cdot s)$
Blade angle*	θ	71.106°
Angle of attack*	β	10°
Velocity x-direction	v_x	12.345 m/s
Velocity y-direction	v_y	78.885 m/s
Mass flow	$\dot{m}$	0.00689 kg/s
Reynolds number	Re	2.08e07

Table A.1: The properties of natural gas. Values provided by OneSubsea is marked by *.

The compressor blade used in this study is non rotating. To imitate the blade rotation the flow into the domain is incoming with an angle. The incoming flow angle, ϕ, is calculated by adding the angle of attack, θ, to the blade angle, β, and is equal to 81.106°. The components of the flow velocity have to be calculated according to this angle. The rotational speed is converted from revolutions per minutes (RPM), ω_{RPM}, to m/s, ω_{grad}, according to

$$\omega_{grad} = \frac{\omega_{RPM} \cdot 2\pi}{60 \cdot D_{hyd}} \tag{A.1}$$

where D_{hyd} is the hydraulic diameter of the blade provided by OneSubsea. The rotational speed in m/s is 78.885 m/s which equals the value of the velocity in the y-direction, v_y. The velocity in x-direction, v_x, is calculated from the flow angle and the rotational speed i.e. $\omega_{grad} \tan(\phi)$. The total velocity in the flow direction is calculated in corresponding way, using the rotational speed and flow angle, i.e. $\omega_{grad} \sin(\phi)$ and is equal to 79.845 m/s.

The mass flow of the natural gas flow, $\dot{m}_{NG}$, is calculated according to

$$\dot{m}_{NG} = \rho v_x A \tag{A.2}$$

where A is the area of the inlet. The value of the mass flow is found in Table A.1.

A.1.2 Oil

The main properties of the oil can be seen in Table A.2.

Variable	Symbol	Value
Density*	ρ_d	700 kg/m^2
Velocity x-direction	v_x	12.345 m/s
Velocity y-direction	v_y	78.885 m/s
Mass flow 1% volume fraction	α_d	0.00152 kg/s
Mass flow 2% volume fraction	α_d	0.00306 kg/s
Reynolds number	Re_d	208 - 41500
Stokes number	St	0.00251 - 100

Table A.2: The properties of oil. Values provided by OneSubsea is marked by *.

The velocity of the droplets was the same as for the natural gas. The mass flow of the oil, $\dot{m}_{oil}$, was calculated from

$$\dot{m}_{oil} = \frac{\alpha_d \dot{m}_{NG}}{1 - \alpha_d} \frac{\rho_d}{\rho_c}. \tag{A.3}$$

The Reynolds number was calculated as defined in (2.14) and the Stokes number as defined by (2.13) where τ_d is

$$\tau_d = \frac{\rho_d D^2}{18\mu_c} \tag{A.4}$$

where D is the particle diameter.

A.2 Coefficient of restitution

The COR is calculated from (2.22) and the Stokes number used is presented in Legendrea et al. [12] and varies with particle diameter. The Stokes number varies

from 514 to 1.03e05. Most of the variables have been defined in Section 2.2.5.1 but those who were not will be discussed here. The density of the gas phase and oil phase are defined in Appendix A Section A.1 and the droplet diameter ranges from 1 µm to 200 µm. The velocity, u_∞ is defined as the initial speed of the particles in the direction of the flow, $78.885/sin(81.106) = 79.845$ m/s. Two decimals were used for the final value of COR, which resulted in values ranging from 0.85 to 0.91, as defined in Table 3.6.

A.3 Mass weighted average velocity angle

In this sections the calculations for the MWAVA are provided. The values presented are from Fluent, since there is not a big difference between the solutions from CFX and Fluent.

Table A.3 provides the values of the average particle flow properties. The velocities in x- and y-direction from each particle size is outputted at the axial clearance and the values were then averaged. The average outflow angle is calculated from these averaged velocities by using trigonometry.

Size [µm]	Average velocity x-direction [m/s]	Average velocity y-direction [m/s]	Average angle [°]
1	13.88	41.46	70.67
5	14.16	43.28	71.70
10	14.50	43.73	71.66
20	14.92	43.32	71.01
30	14.92	43.35	71.02
40	14.82	43.79	71.31
50	14.87	44.26	71.43
60	15.18	44.67	71.23
70	15.47	44.93	71.01
80	15.71	44.98	70.78
90	16.04	44.81	70.32
100	16.86	44.20	69.09
110	17.83	44.22	67.99
120	18.38	42.88	66.67
130	19.47	42.56	65.26
140	19.58	42.04	64.82
150	20.11	41.33	63.81
160	21.01	41.09	62.70
170	21.13	41.08	62.52
180	21.67	41.90	62.24
190	22.59	41.27	60.88
200	22.15	39.57	60.11

Table A.3: Average velocity in x- and y-direction and average velocity angle for different particle sizes. The values are calculated from data outputted from Fluent.

From the averaged particle velocity angle ϕ_d and the average velocity angle of natural gas ϕ_c the MWAVA is calculated by (4.1). The MWAVA for different particle sizes is presented in Table A.4. The values in the table are visually presented in Figure 4.8.

Size [μm]	Average angle - Natural gas	MWAVA - oil - 1% volume fraction	MWAVA - oil - 2% volume fraction
1	72.10	72.08	72.07
5	72.10	72.09	72.09
10	72.10	72.09	72.09
20	72.10	72,09	72.07
30	72.10	72.09	72.07
40	72.10	72.09	72.08
50	72.10	72.09	72.08
60	72.10	72.09	72.08
70	72.10	72.09	72.07
80	72.10	72.08	72.07
90	72.10	72.08	72.06
100	72.10	72.07	72.04
110	72.10	72.06	72.01
120	72.10	72.04	71.99
130	72.10	72.03	71.96
140	72.10	72.02	71.95
150	72.10	72.01	71.93
160	72.10	72.00	71.90
170	72.10	72.00	71.90
180	72.10	71.99	71.89
190	72.10	71.98	71.87
200	72.10	71.98	71.86

Table A.4: Average angle for natural gas and MWAVA for 1% and 2% oil droplet volume fraction, for each particle size.

A.4 Compare case

In the Compare case the droplets velocity in x-direction, location in x- and y-direction and the normal wall distance was outputted from CFX. The data represents each particle track, tracked in each node of the computational grid. To be able to find out the droplets distance from the wall at the point where the rebound of the droplets is no longer dominant, i.e. the droplets are flowing in the same direction as the natural gas flow, the velocity components that have their value in the same direction as the gas flow, i.e. plus x-direction, are filtered out. What is left are the droplets that rebound with the wall but since it is not possible to output droplet ID in CFX it is not clear where the switch between particle tracks is. For that a marker was put to those points that started at the inlet and the data between those points analysed by only using the point that is furthest from the wall. The wall distance for that point is then divided by the tube diameter to get a normalised distance as used by Tu et al. [14]. The average value of the normalised wall distance for all rebound droplets for each case was then used to represent one point in Figure 4.12.

B
Figures

This section presents some complementing figures that were not presented in the results. It also provides the graphs produced from the solution process, presenting the monitors used and value for y^+ along the blade.

B.1 Particle tracks for comparison

In the results for the Wall film the particle tracks for a 100 µm droplet injection is presented. In Figure B.1 the particle tracks from the equivalent injection in the Base case is presented.
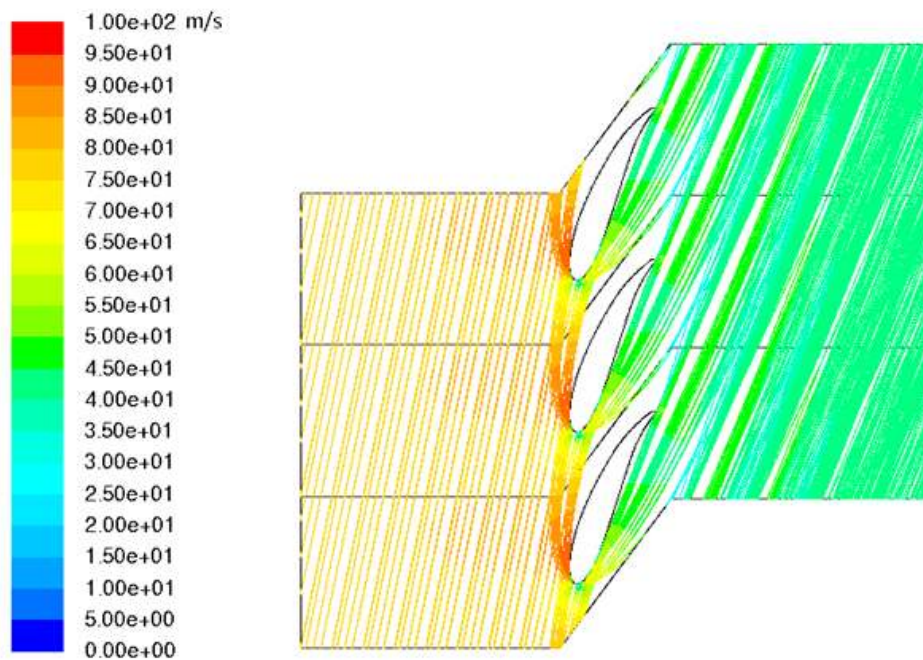

Figure B.1: Particle tracks, from the Base case, colored by velocity magnitude for droplets with 100 µm diameter.

B.2 Solution strategy

This section presents the graphs from the solution process in Fluent and CFX. The convergence for the monitors used is presented.

B.2.1 CFX

When deciding if the natural gas flow has converged three monitors where observed; momentum and mass, drag and lift, and mass imbalance. Once the momentum and mass have stabilised the other monitors are observed to see if the solution has converged. If drag and lift are constant and the mass imbalance does not oscillate significantly the solution is considered to be converged. These three monitors for the simulation of natural gas can be seen in Figure B.2, Figure B.3 and Figure B.4. The natural gas flow simulation was said converged after 90 iterations.
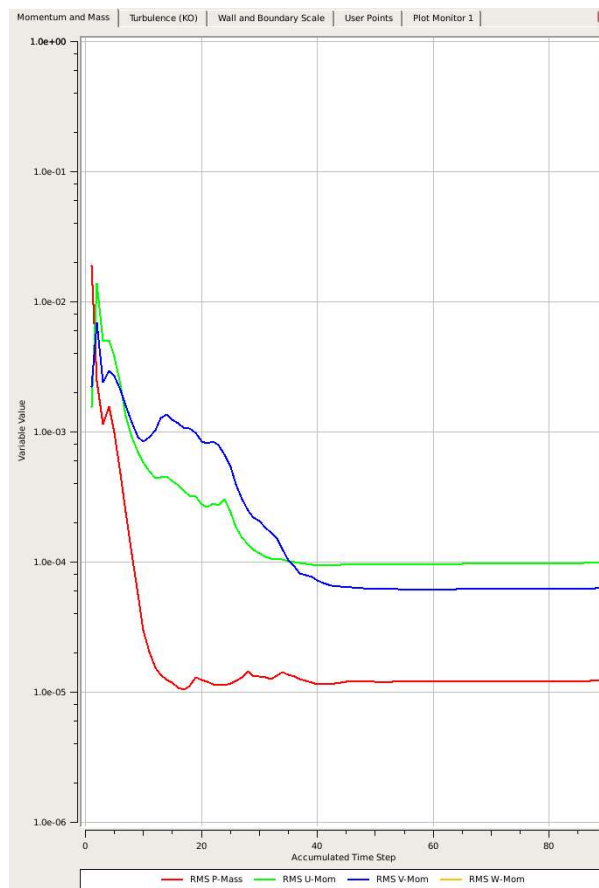

Figure B.2: Momentum and mass residuals monitor for CFX simulation of natural gas. The residuals have stabilised which indicates convergence.
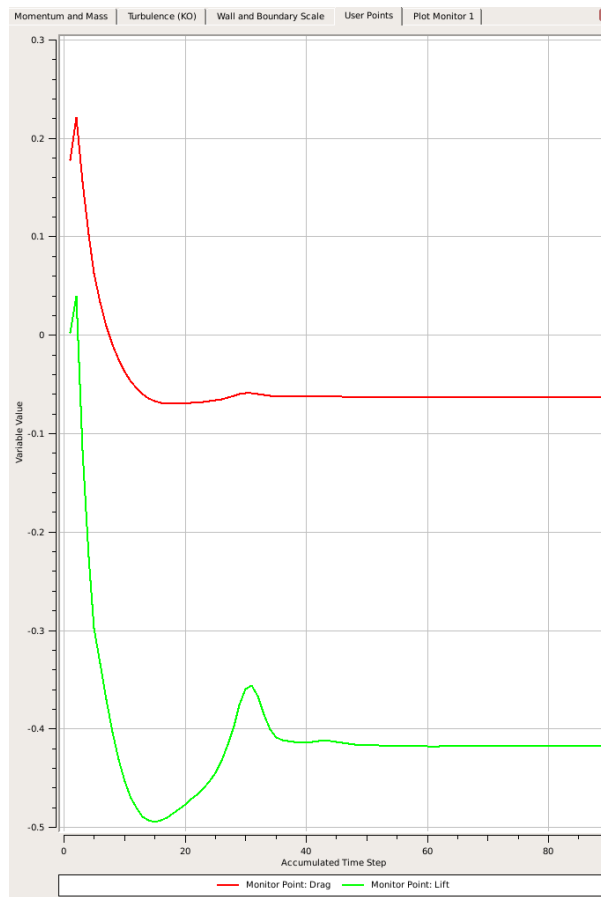
Figure B.3: The drag and lift monitor for the natural gas simulation in CFX. Stabilised values indicate convergence. The monitors have stabilised which indicates convergence.
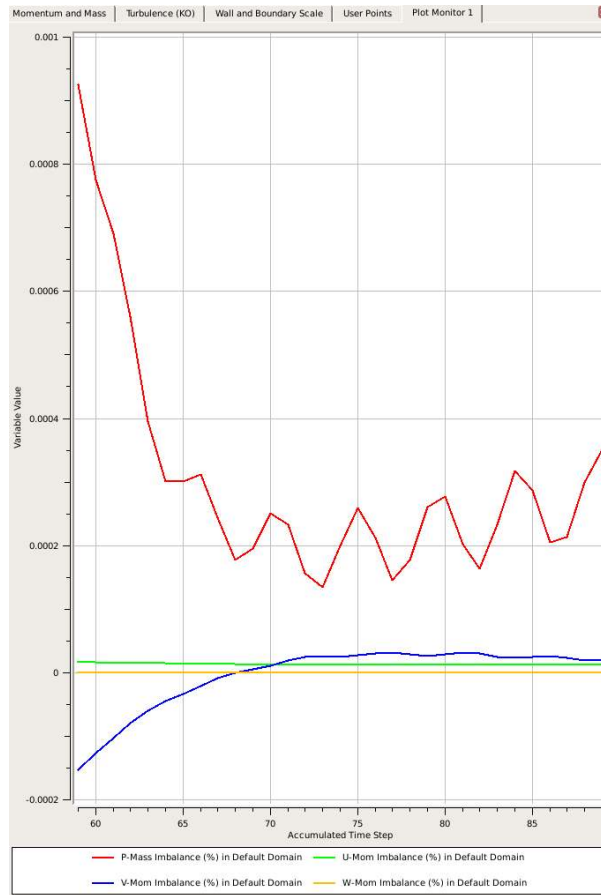
Figure B.4: Mass imbalance monitor for natural gas simulation in CFX. Small oscillations indicate convergence. Note that the scale shows only the last 30 iterations and the y-axis scale is small and therefore this can be said to be converged.

B.2.2 Fluent

In Fluent the convergence was concluded mainly by observing the residuals. Once the residuals had reached a constant value the solution was concluded to have converged. This occurred around 700 iterations. A typical look of the residuals is presented in Figure B.5. The initial fluctuations are caused by stepwise increase of the flow Courant number and explicit relaxations factors, that was performed to assure convergence.
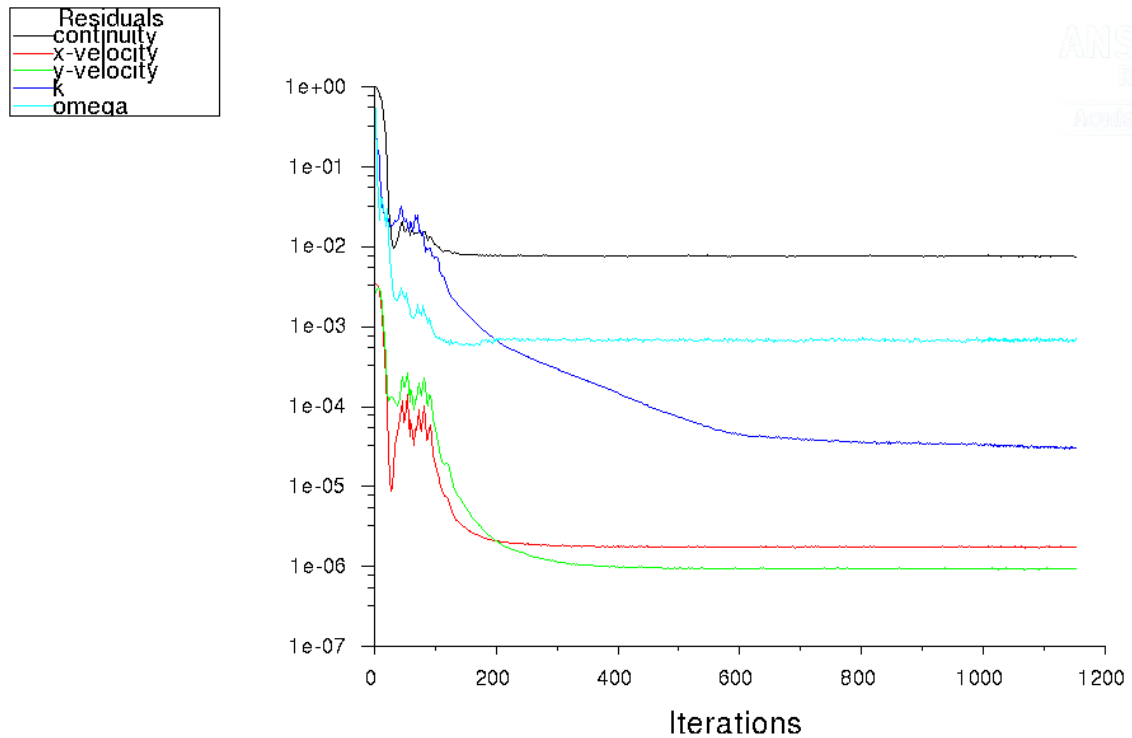

Figure B.5: Mass imbalance monitor for natural gas simulation in Fluent. The residuals have stabilised which indicates convergence.